AD-A087 553 NORTHWESTERN UNIV EVANSTON IL DEPT OF CHEMISTRY F/G 7/3
CHEMICAL, SPECTRAL, STRUCTURAL, AND CHARGE TRANSPORT PROPERTIES--ETC(U)
JUL 80 R P SCARINGE, C J SCHRAMM N00014-77-C-0231
UNCLASSIFIED TR-11 NL

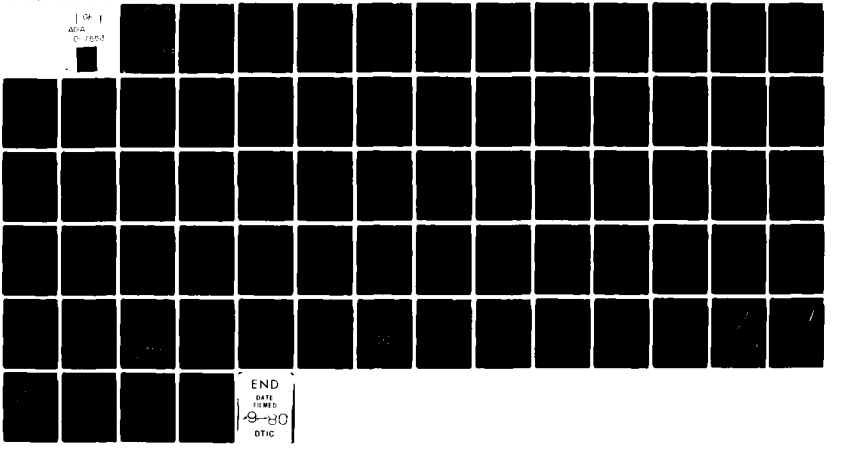

END
DATE FILMED
9-80
DTIC

OFFICE OF NAVAL RESEARCH

Contract N00014-77-C-0231

Task No. NR 053-640

TECHNICAL REPORT NO. 11

Chemical, Spectral, Structural, and Charge Transport Properties Of The Molecular Metals Produced By Iodination Of Nickel Phthalocyanine

by

Raymond P. Scaringe, Charles J. Schramm, Djordje R. Stojakovic, Brian M. Hoffman, James A. Ibers, and Tobin J. Marks

TR-11

11 Jul 80

Prepared for Publication

in

The Journal of the American Chemical Society

Northwestern University
Department of Chemistry
Evanston, Illinois 60201

July 17, 1980

Unclassified

SECURITY CLASSIFICATION OF THIS PAGE (When Data Entered)

REPORT DOCUMENTATION PAGE		READ INSTRUCTIONS BEFORE COMPLETING FORM
1. REPORT NUMBER Technical Report No. 11	2. GOVT ACCESSION NO. AD-A084 533	3. RECIPIENT'S CATALOG NUMBER
4. TITLE (and Subtitle) Chemical, Spectral, Structural, and Charge Transport Properties of the "Molecular Metals" produced by Iodination of Nickel Phthalocyanine		5. TYPE OF REPORT & PERIOD COVERED Interim, 1980 6. PERFORMING ORG. REPORT NUMBER
7. AUTHOR(s) Raymond P. Scaringe, Charles J. Schramm, Djordje R. Stojakovic, Brian M. Hoffman, James A. Ibers, and Tobin J. Marks		8. CONTRACT OR GRANT NUMBER(s) N00014-77-C-0231
9. PERFORMING ORGANIZATION NAME AND ADDRESS Northwestern University Department of Chemistry Evanston Illinois 60201		10. PROGRAM ELEMENT, PROJECT, TASK AREA & WORK UNIT NUMBERS NR-053-640
11. CONTROLLING OFFICE NAME AND ADDRESS		12. REPORT DATE July 17, 1980 13. NUMBER OF PAGES 66
14. MONITORING AGENCY NAME & ADDRESS(if different from Controlling Office)		15. SECURITY CLASS. (of this report) unclassified 15a. DECLASSIFICATION/DOWNGRADING SCHEDULE

16. DISTRIBUTION STATEMENT (of this Report)

Approved for public release; distribution unlimited

17. DISTRIBUTION STATEMENT (of the abstract entered in Block 20, if different from Report)

18. SUPPLEMENTARY NOTES

19. KEY WORDS (Continue on reverse side if necessary and identify by block number)

Polyiodide
Conductive Material
Mixed valence material
Phthalocyanine
Organic conductor
Molecular Metal

20. ABSTRACT (Continue on reverse side if necessary and identify by block number)

This paper presenta a detailed study of the solid state chemical, spectral, structural, and charge transport properties of the materials which result from treating nickel phthalocyanine (NiPc) with elemental iodine. A range of $NiPcI_x$ stoichiometries is obtained where x=0 to ca. 3.0; electrical conductivities of compressed polycrystalline samples are comparable with those of other "molecular metals." Single crystals were obtained for $NiPcI_{1.0}$. These crystallize in the space group D_4^2 h-P4/mcc, with two formula units in a

DD FORM 1 JAN 73 1473 EDITION OF 1 NOV 65 IS OBSOLETE S/N 0102-014-6601 |

Unclassified

SECURITY CLASSIFICATION OF THIS PAGE (When Data Entered)

unit cell having dimensions $\underline{a}$ = 13.936(6), $\underline{c}$ = 6.488(3)Å. Full matrix least-squares refinement of 65 variables gave a final value of the conventional R index (on F) of 0.042 for 375 reflections having $F_o^2 > 3\sigma(F_o^2)$. The crystal structure consists of stacked, planar NiPc units (staggered by 39.5°) and disordered chains of iodine atoms extending in the $\underline{c}$ direction. The NiPc units have crystallographically imposed symmetry 4/m. The interplanar Ni-Ni separation is 3.244(2)Å, and the intramolecular Ni-N distance, 1.887(6)Å. Analysis of the diffuse scattering pattern arising from disordered iodine chains reveals that iodine is present as I_3^-. An I-I distance of 3.00 and a I...I distance of 3.72Å are derived from the diffuse scattering. Resonance Raman and iodine-129 Mössbauer spectroscopic measurements indicate that iodine that iodine is present predominatly if not exclusively as I_3^- for all $NiPcI_x$ where $x \leq 3$. Optical spectroscopic and X-ray powder diffraction studies of the $x \neq 1.0$ phases suggest that mixtures of several discrete phases are present. Single crystal electron spin resonance studies (epr) of $NiPcI_{1.0}$ reveal that the iodine oxidation is ligand-centered yielding π-radical cations. The charge distribution thus can best be represented as $[Ni^{II}Pc]^{+0.33}(I_3^-)_{0.33}$ although there is ca. 0.002 unit of charge back-transferred from each I_3^- unit to the metallomacrocycle stack. Susceptibility measurements by epr ans static techniques can be interpreted in terms of a narrow bandwidth metal (ca. 0.24 eV) and a significant contributions from van Vleck paramagnetism. The electrical conductivity of $NiPcI_{1.0}$ crystals has been investigated by four-probe techniques. Room temperature conductivities along the crystallographis stacking direction are in the range 260-750 $\Omega^{-1}cm^{-1}$ and carrier mean free paths are in the range 3.3-8.2 Å. The temperature dependence of the conductivity is metallic ($\rho \sim T^{1.7 \pm 0.2}$) down to ca. 55° K, at which point there occurs an abrupt reduction in conductivity. Neither the resonance Raman of the I_3^-, the epr linewidth, nor the magnetic susceptibility is sensitive to this transition.

Contribution from
the Department of Chemistry and
the Materials Research Center
Northwestern University
Evanston, Illinois 60201

CHEMICAL, SPECTRAL, STRUCTURAL, AND CHARGE TRANSPORT PROPERTIES OF THE "MOLECULAR METALS" PRODUCED BY IODINATION OF NICKEL PHTHALOCYANINE

Raymond P. Scaringe, Charles J. Schramm, Djordje R. Stojakovic,
Brian M. Hoffman,* James A. Ibers,* and Tobin J. Marks*,[1]

ABSTRACT

This paper presents a detailed study of the solid state chemical, spectral, structural, and charge transport properties of the materials which result from treating nickel phthalocyanine (NiPc) with elemental iodine. A range of $NiPcI_x$ stoichiometries is obtained where x = 0 to ca. 3.0; electrical conductivities of compressed polycrystalline samples are comparable with those of other "molecular metals." Single crystals were obtained for $NiPcI_{1.0}$. These crystallize in the space group D_{4h}^2-P4/mcc, with two formula units in a unit cell having dimensions $\underline{a}$ = 13.936(6), $\underline{c}$ = 6.488(3) Å. Full-matrix least-squares refinement of 65 variables gave a final value of the conventional R index (on F) of 0.042 for 375 reflections having $F_o^2 > 3\sigma(F_o^2)$. The crystal structure consists of stacked, planar NiPc units

(staggered by 39.5°) and disordered chains of iodine atoms extending in the c direction. The NiPc units have crystallographically imposed symmetry 4/m. The interplanar Ni-Ni separation is 3.244(2)Å, and the intramolecular Ni-N distance, 1.887(6)Å. Analysis of the diffuse scattering pattern arising from disordered iodine chains reveals that iodine is present as I_3^-. An I-I distance of 3.00 and a I···I distance of 3.72 Å are derived from the diffuse scattering. Resonance Raman and iodine -129 Mössbauer spectroscopic measurements indicate that iodine is present predominantly if not exclusively as I_3^- for all $NiPcI_x$ where $x \leq 3$. Optical spectroscopic and X-ray powder diffraction studies of the $x \neq 1.0$ phases suggest that mixtures of several discrete phases are present. Single crystal electron spin resonance studies (epr) of $NiPcI_{1.0}$ reveal that the iodine oxidation is ligand-centered yielding π-radical cations. The charge distribution thus can best be represented as $[Ni^{II}Pc]^{+0.33}(I_3^-)_{0.33}$, although there is ca. 0.002 unit of charge back-transferred from each I_3^- unit to the metallomacrocycle stack. Susceptibility measurements by epr and static techniques can be interpreted in terms of a narrow bandwidth metal (ca. 0.24 eV) and a significant contribution from van Vleck paramagnetism. The electrical conductivity of $NiPcI_{1.0}$ crystals has been investigated by four-probe techniques. Room temperature conductivities along the crystallographic stacking direction are in the range 260-750 $\Omega^{-1}cm^{-1}$, and carrier mean free paths are in the range 3.3-8.2 Å. The temperature dependence of the conductivity is metallic ($\rho \sim T^{1.9 \pm 0.2}$) down to ca. 55 °K, at which point there occurs an abrupt reduction in conductivity. Neither the resonance Raman of the I_3^-, the epr linewidth, nor the magnetic susceptibility is sensitive to this transition.

Present experience indicates that for a coordination compound to form an electrically conductive molecular crystal, two criteria are highly desirable, if not essential. First, the metal-ligand molecules must be arrayed in close communication and in crystallographically similar environments. Second, the metal-ligand complex must adopt a non-integral formal oxidation state.[2] The latter characteristic has been referred to as "partial oxidation", "mixed valence", or "incomplete charge transfer", and although this state has generally been effected with oxidizing agents, in principle it could equally well be achieved by a partial reduction. The highly conductive coordination compounds studied to date, as exemplified by the tetracyanoplatinate materials, represent a class of materials in which transport properties can be understood almost completely in terms of the charge carriers being confined to a conducting spine of metal atoms.[2] The coordinated ligands (e.g., CN^-) are essential in dictating the structural and electronic properties of the metal atom chain, but appear to play little or no direct role in the charge transport process.

Mixed-valent coordination complexes of an entirely different variety are represented by a growing number of partially oxidized materials containing metal complexes of planar, conjugated organic ligands.[3-5] Especially in the case of iodine oxidants, it is possible to synthesize broad classes of non-integral oxidation state materials, and furthermore, using resonance Raman,[5] iodine Mössbauer,[5] as well as diffuse X-ray scattering techniques,[6] to identify the form of iodine present (I_2, I^-, I_3^-, I_5^- or mixtures thereof), hence the degree of incomplete charge transfer. Among the known classes of

partially oxidized metallomacrocycles, the metallophthalocyanines (MPc)[3] stand out in terms of charge transport properties, chemical flexibility, and technological accessibility.

We have previously shown that iodine oxidation of a variety of metallophthalocyanines (as well as the metal-free derivatives) produces an extensive new class of highly conductive (as judged by measurements on compressed polycrystalline samples) molecular materials with a wide range of dopant stoichiometries (eq. (1)).[3a] Subsequently we reported preliminary

$$MPc + x/2\ I_2 \rightleftharpoons MPc(I)_x \qquad (1)$$

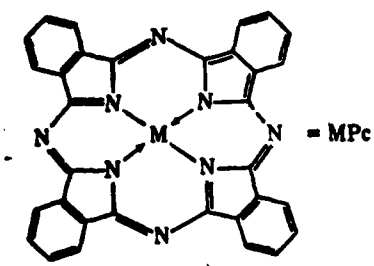

M = Fe, Co, Ni, Cu, Pt, H_2

single crystal studies on $NiPcI_{1.0}$, which demonstrate that it is a "molecular metal" down to 55 °K and that carrier mean free paths compare favorably with those of the most conductive stacked molecular materials known.[3b] In the present study, we focus in depth on the properties of the $NiPcI_{1.0}$ and $NiPcI_x$ materials. This includes X-ray diffraction, optical, resonance Raman, iodine Mössbauer, electron spin resonance, magnetic susceptibility, and charge transport measurements. It is seen that the iodinated

nickel phthalocyanines are indeed "molecular metals". In the case of $NiPcI_{1.0}$ single crystals, the crystal structure has been precisely characterized as stacks of $NiPc^{+0.33}$ units and parallel chains of I_3^- counterions with a disorder among these latter chains. The electrical conductivity in the stacking direction is metallic down to 55 °K, and this interpretation is supported by essentially constant magnetic susceptibility. At ca. 55 °K, $NiPcI_{1.0}$ undergoes a metal-semi-conductor transition; this transition does not manifest itself in the resonance Raman spectrum, nor, surprisingly, in the magnetic susceptibility or esr linewidth.

In subsequent phthalocyanine contributions we will explore the effects of metal ion and ligand modification upon the electronic and strutural properties.

EXPERIMENTAL

Nickel phthalocyanine was purchased from Eastman Kodak Co. and was sublimed at 400 °C/10^{-3} torr before use. Solvents were of analytical reagent or spectrograde quality. Elemental analyses were performed by Micro-Tech Laboratories, Inc., Skokie, Illinois, or by Miss H. Beck, Northwestern Analytical Services Laboratory.

Synthesis of $NiPcI_x$ Materials. To prepare polycrystalline samples of various stoichiometries, finely powdered nickel phthalocyanine was stirred in a closed vial with various amounts of iodine in chlorobenzene for 48 hr. Longer reaction times produced no detectable changes in spectral or transport properties. The iodinated nickel phthalocyanine was collected by centrifugation, washed with several portions of hexane, and dried under a stream of dry nitrogen. Relevant synthetic information and analytical data

are compiled in Table I. Single crystals of $NiPcI_{1.0}$ were grown in an H-tube by diffusing together solutions of iodine and NiPc in either 1,2,4-trichlorobenzene or 1-chloronaphthalene.

Anal. Calcd. for $C_{32}H_{16}I_{1.0}N_8Ni$: C, 55.02; H, 2.31; N, 16.04; I, 18.17. Found: C, 54.61; H, 2.34; N, 16.09; I, 18.37.

X-ray Diffraction Study of $NiPcI_{1.0}$. Single crystals of this material were grown as described above. On the basis of a series of Weissenberg and precession photographs the crystals were assigned to Laue group 4/mmm of the tetragonal system. The only systematic absences observed were for $0k\ell$ and $hh\ell$ with ℓ odd; hence the space group is either P4/mcc or P4cc. Excellent agreement among Friedel pairs and successful refinement of the structure support the choice of space group D_{4h}^2-P4/mcc. The cell constants of $\underline{a}$ = 13.936(6), $\underline{c}$ = 6.488(3) Å were obtained by usual procedures[7] using the setting angles on a FACS-I diffractometer of 15 hand-centered reflections having 2θ (Cu $K\alpha_1$) $\geq 30°$. The observed density of 1.78(4)g/cm^3, obtained by flotation of the crystals in $ZnBr_2$ solutions, may be compared with that of 1.84 g/cm^3 calculated for two formula units in the cell.

Although most crystals examined exhibited Bragg peaks with considerable structure, the small specimen selected for data collection displayed only slight splittings. Data were collected at room temperature using Cu $K\alpha$ radiation prefiltered with 1 mil Ni foil by methods standard in this laboratory.[7] Crystal data and details of collection of Bragg peak intensity data are summarized in Table II.

Laue and oscillation photography displayed the presence of diffuse scattering in addition to normal Bragg scattering. Diffuse scattering was

confined to planes perpendicular to the c^* axis with a spacing (c'^*) between such planes being $2c^*/3$. Except for superstructure reflections the intensity within each plane falls off smoothly with increasing scattering angle, but it changes markedly from one layer to the next. In particular, no diffuse layers with $\ell = 3n$ were observed.

The relative intensities of the diffuse layers were obtained by X-ray counter techniques employing Cu Kα radiation and a graphite monochromator. The sample area was enclosed in a polyethylene bag filled by a constant flow of helium to reduce atmospheric scattering. The crystal used was not the one employed for collection of Bragg peaks but rather was a needle of octagonal cross section approximately 0.8 mm long and with separations of 0.06 mm between opposite axial faces. Reciprocal space was sampled point by point along a line perpendicular to the diffuse planes. Since no diffuse layers with $\ell' = 3n$ were observed photographically, intensity data were not gathered for these layers. Data were collected out to the limit of the Cu sphere, which corresponds to $\ell' = 11$. Counting times for each point ranged from 600 to 2000 seconds. Peak and background points were separated by examining plots of the data. Intensities were corrected for polarization, geometrical factors, and absorption.[8,9]

Solution and Refinement of the Structure

An origin-removed sharpened Patterson function indicated that all iodine atoms were at relative positions $\pm 1/2$, $\pm 1/2$, $\pm 1/4$ from the nickel atoms. Many of the iodine to ring atom vectors were evident at $w = 1/4$, leading to the correct orientation of the ring and the relative positions of most of

the light atoms. The orientation of the chelate ring with respect to the crystallographic axes precluded the possibility of site symmetry 422 for the nickel atom. With the added constraint Z = 2, site symmetry 4/m was the only remaining possibility in P4/mcc. Initial refinements were carried out on F_o, using the 375 unique reflections having $F_o^2 > 3\sigma(F_o^2)$. After idealizing the ring atom positions obtained from the vector map, one cycle of least-squares refinement with variable isotropic thermal parameters resulted in values of 0.125 and 0.161, respectively, for R and R_w, the usual agreement indices. Two cycles of refinement with variable anisotropic thermal parameters for all non-hydrogen atoms reduced those values to 0.058 and 0.074, respectively. The subsequent difference Foureir map indicated the positions of all hydrogen atoms and also one small peak ($\sim$1.0 $e\text{Å}^{-3}$) located about 1 Å from the iodine position along the z axis. All hydrogen atoms were found to be close to their idealized position (C-H = 0.95Å); these positions were used and not varied in the least-squares process for the remainder of the refinement. Each hydrogen atom was assigned a fixed isotropic thermal parameter equal to 1 Å^2 greater than that of the carbon atom to which it is bonded. In the final cycle of refinement on $|F_o|$, there were 375 observations and 65 variables and the resultant values of R and R_w were 0.043 and 0.051, respectively. No positional parameters exhibited a significant shift during this cycle.

Two additional cycles of refinement of F_o^2 (including $F_o^2 < 0$) increased the number of available observations to 630 and resulted in the expected decrease in the estimated standard deviation of all variables. In this

first cycle of refinement the occupancy factor of the iodine was also allowed to vary yielding a value of 0.995(6) iodine atoms per site; in the final cycle the occupancy was fixed at one iodine per site. The final cycle of least-squares refinement then involved full-matrix refinement of 65 variables with 630 observations; the final values of R and R_w (on F_o^2) are 0.057 and 0.113, respectively. The R index on F_o for those reflections having $F_o^2 > 3\sigma(F_o^2)$ is 0.042. With the exception of one small peak (0.7 $e\text{Å}^{-3}$) at the Ni position and several small peaks (0.5 - 0.6 $e\text{Å}^{-3}$) along the iodine chain the final difference Fourier synthesis is featureless. The final positional and thermal parameters are given in Table III, root-mean-square amplitudes of vibration in Table IV.[10] A listing of structure amplitudes is available.[10] A minus sign preceding $|F_o|$ indicates a negative value for F_o^2.

Resonance Raman Measurements. Spectra were recorded on a 0.85 m Spex 1401 double monochromator spectrometer using 5145Å Ar^+ excitation. Samples were studied in spinning (1800 rpm) 5 or 12 mm Pyrex tubes using a 180° backscattering illumination geometry. A number of scans were made of each sample (the first at lowest possible laser power) to check for possible sample decomposition. Spectra were calibrated with the exciting line (ν_0) or laser plasma lines. Low temperature studies were performed with the apparatus described previously.[5b,11]

Electronic Spectroscopy. Optical spectra were recorded on a Cary 17D spectrophotometer. Solid samples were examined as Nujol mulls between quartz plates. Several scans were made of each sample to check for possible decomposition.

X-Ray Powder Diffraction Measurements. Samples were studied using a Philips Electronic Instruments Model XRG-5000 powder diffractometer with a pyrollitic graphite monochromator in the diffracted beam geometry and Cu Kα radiation. Samples were examined as 4.5 x 39 mm pressed pellets. Data were collected at a scan rate of 0.25°/min. and recorded on a strip-chart recorder.

Iodine-129 Mössbauer Spectroscopy. The sample was prepared by the reaction of NiPc in chlorobenzene with $^{129}I_2$ prepared as described previously. Elemental analysis showed it to be of stoichiometry $NiPcI_{2.16}$. The Mössbauer spectrometer was that described elsewhere ($^{66}Zn^{129}Te$ source, standard transmission geometry, ^{57}Fe calibrated velocity generated by a feedback-controlled vibrator with sinusoidal acceleration[5b,11]). The absorber was prepared by thoroughly powdering the $NiPcI_{2.16}$ material and diluting it with boron nitride. Both source and absorber were maintained at 4.2 °K during data acquisition. Data were collected with a proportional counter and 400 channel multichannel analyzer operating in the time mode. Data processing utilized the program GENFIT,[12a] which finds the optimum isomer shifts, quadrupole coupling constants, linewidths, site populations, and asymmetry parameters via non-linear least-squares minimization of the difference between the calculated and observed spectrum. The goodness of fit is judged by the previously defined parameter "Misfit".[12,13]

Electron Spin Resonance Studies. Measurements were carried out using a highly modified Varian E-4 X-band esr spectrometer, with 100 kHz field modulation. Temperatures in the range 300 °K to 90 °K were obtained by regulation of the flow rate of cooled liquid nitrogen boiloff gas. A calibrated copper-constantan thermocouple placed within 1.0 cm of the sample monitored the temperature to within ±1 °K. The extended temperature range

300 °K to 15 °K was obtained with an Air Products LTD-3 cryostat system using liquid helium. The temperature, stable to better than ±1 °K, was monitored by a calibrated rhodium-gold thermocouple placed in the immediate vicinity of the sample.

For the g-tensor measurements, 2,2-diphenyl-1-picrylhydrazyl (DPPH, g = 2.0036) was used to provide absolute field calibration. The cavity resonance frequency was measured to an accuracy of 5 ppm by a transfer oscillator technique.

The sample crystals of $NiPcI_{1.0}$ were mounted on a Teflon crystal holder with silicone grease and then the holder pressed into a piece of quartz tubing. This was attached to a rotating goniometer head of standard design mounted firmly to the resonance cavity. Rotation angles could be measured to a precision of ±1.0°.

The integrated esr intensity was obtained by electronically integrating the first derivative signal and then measuring the area under the absorption curve. For these approximately Lorentzian signals, scans of 20 times the linewidth were run; this limits the error caused by truncation to less than 5%.[14] The relative esr intensities were obtained for temperature dependent studies and were scaled to the appropriate absolute value of the room temperature spin susceptibility, χ^s.

DPPH, Aldrich 99% reagent grade, was used as the standard for determination of absolute spin concentration on the assumption that it exhibited a signal resulting from one spin per molecule. The DPPH employed had a melting point of 136° - 138° C and is thus DPPH(II), which has a susceptibility at 298 °K of 1.13×10^{-3} emu/mole.[15] The DPPH was dispersed in potassium bromide for ease of handling and to achieve a spin concentration per sample size more

characteristic of those found in the iodine oxidized nickel phthalocyanines. Samples were packed in short quartz capillaries to a length of approximately 0.5 cm. Weights of samples were measured to an accuracy of 0.05 mg. The short tube was placed into a larger quartz tube and then into the resonance cavity. The small sample was centered in the cavity. Small sample size and careful positioning ensured that the instrument response was a function of the entire sample for each sample measured.

Static Magnetic Susceptibility Studies. These measurements were performed by the Faraday method using $HgCo(SCN)_4$ as a calibrant. Susceptibility studies over the temperature range 77 °K to 300 °K were obtained by cooling the sample-containing dewar vessel to liquid nitrogen temperature (77 °K) and allowing it to warm slowly to room temperature. As before, temperatures were measured to an accuracy of ±1 °K using a calibrated copper-constantan thermocouple.

Conductivity Studies on Polycrystalline Samples. Electrical conductivity data on polycrystalline $NiPcI_x$ samples were acquired with a four-probe van der Pauw apparatus.[16] Samples were prepared by pressing powders under 3 kbar pressure into cylindrical pellets, 12 mm in diameter and ca. 1 mm thick.

Single Crystal Electrical Conductivity Studies. Electrical contact to crystals mounted for four probe measurements was made with a palladium paint prepared locally. The crystals were mounted in integrated circuit cans prepared as described elsewhere.[17] Most crystals were mounted using 0.001 inch diameter aluminum wire but in some cases 0.0005 inch nickel wire was used. The coefficient of thermal expansion of Ni is half that of Al, and thus the smaller wire should place less strain on a crystal. A four probe low frequency ac technique, described previously, was employed for measuring the sample resistance, and the temperature was measured using a copper-constantan thermocouple located within a few millimeters of the sample.[17]

Temperatures in the range 85 °K to 295 °K were obtained with cold N_2 gas; the extended range 20 °K to 295 °K was achieved with cold helium gas obtained from liquid helium boil off.

The conductivity along the stacking direction of a crystal ($\sigma_{||}$), is defined in terms of a measured resistance, ($R_{||}$), crystal cross-sectional area (A), and distance between voltage probes (L): $\sigma_{||} = L/(R_{||}A)$. Dimensions of crystals mounted for conductivity studies were obtained with a Gaertner toolmakers microscope whose stage movement in the x-y plane is calibrated to ±0.002 mm. On the average, crystals were 0.02 mm in the maximum cross-sectional dimension (w) and 2.0 mm in length; L was typically 0.7 mm. The crystals assume a variety of cross-sectional shapes and their small size precludes an accurate determination of A for a mounted crystal. The value $\tilde{A} = w^2$ necessarily gives an overestimate of A and the two values have been judged to have the relationship $A \approx (0.85 \pm 0.15)\,\tilde{A}$. There is an additional uncertainty in A, because of the error in w from the microscopic measurement itself, which is estimated to be $\Delta w/w \sim \pm 0.1$. The intercontact length (L) can be measured with more accuracy: $\Delta L/L \sim 0.03$. Thus we estimate an overall uncertainty in the cross-sectional area of $\Delta A/A \sim \pm 0.4$. The compounded uncertainties in the crystal dimensions and crystal habit lead to an estimated uncertainty in the absolute conductivity of $\Delta\sigma/\sigma \sim \pm 0.4$. Relative conductivities for a particular crystal at different temperatures are, of course, accurate to the resistance measurement (±1%).

RESULTS

In this section we begin with a discussion of the chemistry and the general properties of $NiPcI_x$ materials as regards mixed valency and transport properties. We then focus in depth on the structural, conductivity, and magnetic properties of $NiPcI_{1.0}$ single crystals. Lastly, using

the single crystal information as a foundation, we discuss the probable nature of the $NiPcI_x$ materials, $x \neq 1$.

NiPc Iodination Chemistry

Nickel phthalocyanine reacts with iodine solutions or vapor according to equation (1) to produce black, polycrystalline solids, $NiPcI_x$, for a wide range of x values (Table I). The iodination reaction is reversible and iodine can be completely removed by heating the material in vacuo. It has also proven possible to grow single crystals of the $NiPcI_x$ compound where x = 1.0 by diffusing together solutions of NiPc and iodine. Crystals of iodinated nickel phthalocyanines could not be produced by exposing NiPc single crystals (grown by sublimation) to iodine solutions or vapor; the formation of a $NiPcI_x$ material was accompanied by visible deterioration and crumbling of the NiPc crystals.

$NiPcI_x$ Resonance Raman Spectroscopy

Figure 1 presents representative solid state resonance Raman spectra in the polyiodide scattering region of two of the $NiPcI_x$ materials. The spectra of the samples with $0 < x <$ ca. 3.0 are identical and exhibit the intense totally symmetric stretching fundamental of I_3^- at 107 cm^{-1} along with the characteristic overtone progression.[5,11,18] There is no evidence of I_5^- ($\nu \approx 160$ cm^{-1}), of I_2 coordinated to donors such as I_3^- ($\nu \approx 180$ cm^{-1}), or of free I_2 ($\nu \approx 200$ cm^{-1}).[5,11,18] Strong scattering from I_3^- is observed when only traces of iodine are present. There was no change in the type of polyiodide as evidenced by the scattering pattern of $NiPcI_{1.0}$ crystals when samples were cooled to 8 °K or heated to 455 °K. At very high iodine levels ($x \gtrsim 3.0$) scattering at 180 cm^{-1}, characteristic of I_2 coordinated to a Lewis

base such as I_3^-, is observed in the $NiPcI_x$ materials (Figure 1). Raman data are compiled in Table V.

The Raman spectrum of NiPc exhibits no scattering in the low frequency region (< 500 cm^{-1}). However, transitions are observed at 592s, 687s, 1140m, 1340s, 1554vs, and 1607m (cm^{-1}). These transitions are analogous to those observed in metalloporphyrins[19] and related tetraazaannulenes;[20,21] they can be assigned to phthalocyanine skeletal modes, probably involving little Ni-N or C-H motion. After partial oxidation of NiPc with iodine, these skeletal modes are still observable, although qualitatively weaker and slightly displaced in energy: 587w, 685w, 1136w, 1340vw, 1550w, 1606m (cm^{-1}); in addition, a new band is observed at 1858 cm^{-1}. Analogous, oxidation state-sensitive metal-ligand "marker" scattering is well known for metalloporphyrins[19] and has been observed in the Raman spectra of partially oxidized metal glyoximates[5b] and tetraazaannulenes.[21]

$NiPcI_x$ Optical Spectra.

In Figure 2 are shown the solid-state optical spectra of NiPc, $NiPcI_{1.0}$, and the compound $(benzamide)_2H^+I_3^-$, which contains linear chains of I_3^- ions[22] as does $NiPcI_{1.0}$ (vide infra). The strong absorptions at 693 and 621 nm in NiPc can be assigned to a ligand-centered π-π^* transition ($a_{1u} \rightarrow e_g$ under D_{4h} symmetry);[23] the multiplicity of the band (a narrow 0-0 and weaker 0-1 transition are seen in solution) has been observed previously and has been attributed to removal of the degeneracy of the e_g level because of lowered symmetry of the crystalline environment.[24] Upon iodination (and change in site symmetry to C_{4h}) the π-π^* transition appears as a singlet at 640 nm. In addition, a new absorption is observed at 530 nm which, on the basis of the strong $(benzamide)_2H^+I_3^-$ band at 510 nm and results on other polyiodides, is attributed to the triodide component. It is no doubt the transition responsible for the resonance-enhanced I_3^- Raman scattering. Optical spectra

of $NiPcI_x$ were also studied as a function of iodine content. For $x < 1$ a shoulder on the 640 nm peak at 693 nm was detected which appears to arise from unoxidized NiPc; this observation will be discussed further in connection with the X-ray powder diffraction data (vide infra). The optical absorption spectra of all materials with $x \geq 1$ are essentially identical.

$NiPcI_x$ Iodine Mössbauer Spectroscopy

The iodine-129 Mössbauer spectrum of $NiPc^{129}I_{2.16}$ is shown in Figure 3. Computer analysis yielded the spectral parameters compiled in Table VI. The spectrum is typical of a symmetrical ($D_{\infty h}$) triiodide.[11,25] There is no evidence of I^- (δ = -0.51 mm/sec, $e^2q^{129}Q$ = 0.00 MHz)[11,26] or I_2 (δ = +0.98 mm/sec, $e^2q^{129}Q$ = 1586 MHz in frozen hexane solution)[11,26] and it is estimated that these species are present to no greater than 3 and 5 mole percent, respectively. Clearly the major, if not exclusive, iodine constituent is symmetrical I_3^-.

$NiPcI_{1.0}$ Single Crystal X-ray Investigation

The structure of $NiPcI_{1.0}$ consists of columnar stacks of NiPc well separated from linear chains of iodine, both running parallel to the z axis. The iodine chains are located in channels defined by the benzo groups of the nearby phthalocyanine ligands. A stereo view of the crystal packing is provided in Figure 4. The packing is considerably different from that in the unoxidized precursor, β-NiPc, in which the metallomacrocycle moieties are arrayed in slipped stacks. The iodine atoms lie on positions of 422 (D_4) symmetry, the NiPc molecule on 4/m (C_{4h}) sites. Owing to the crystallographically imposed 4/m symmetry, the NiPc molecule is rigorously constrained to be planar. Of the numerous metallophthalocyanine structures reported to date[27-38] this compound is the first to have this crystallographic

requirement. The Ni-N(1) distance of 1.887(6) Å is similar to that observed in a number of four-coordinate phthalocyanine complexes of first-row metals.[39] Allowing for the fact that the radius of the central hole of a phthalocyanine ring is about 0.11 Å smaller than that of a porphyrin molecule, this separation is also in agreement with the suggestion by Hoard[40] that radial strain is minimized in metalloporphyrins when the M-N separation is ~2.01 Å. A perspective view of the molecule, together with the labeling scheme, is given in Figure 5. Bond lengths and angles are compiled in Table VII. The bond lengths and angles reported here are similar to those of previously reported phthalocyanine complexes.[27-38,41] For a quantitative comparison the chemically distinct bonds have been averaged in accordance with D_{4h} symmetry and these values are given in Table VIII with similarly averaged data from a number of recent structural reports.[41] $NiPcI_{1.0}$ is in all respects similar to those previously reported, and evidently partial oxidation has had no measurable effect on the dimensions of the phthalocyanine ring. The average bond lengths and angles correspond well to the Kekule formula given above Table VIII, where the N_m-C_a, N-C_a, and C_a-C_b linkages are assigned π bond order of 1/2, 1/4, and 1/4, respectively. The average values for N_p-C_a and C_a-C_b of 1.376(10) Å and 1.453(3) Å are also in good agreement with the values 1.379(6) Å and 1.443(5) Å observed for metalloporphyrins.[42] As noted previously the C_a-N_m-C_b angle is slightly contracted relative to the C_a-C_m-C_b angle in the porphyrin analogues but the effect is not as large as originally thought. This contraction has been attributed to the steric requirements of the lone pair electrons on atom N_m. All bond lengths in the fused benzene ring are found to be equivalent: their average value of 1.392(6) Å compares well with the value for benzene.

It is evident however that not all angles within the fused benzene ring are equivalent, the average C_b-C_c-C_d angle being significantly compressed at 117.3(2)° as compared with the others which are found to be equivalent at 121.4(2)°. This effect has been noted previously,[27,33] but is not peculiar to the phthalocyanine macrocycle. The same effect is observed frequently in hydrocarbon structures and has been attributed to strain resulting from fusion with a five membered ring.[43]

The crystal packing in $NiPcI_{1.0}$ is similar to that reported for the partially oxidized metallomacrocyclic systems $Ni(dpg)_2I$ (dpg = diphenylglyoximato),[3b] Ni(OMTBP)I (OMTBP = octamethyltetrabenzoporphyrinato),[4a,d] Ni(tetrabenzporphyrin)I,[44] and $M(bqd)_2I_{0.5}\cdot 1/2S$ (M = Ni, Pd, bqd = 1,2-benzoquinonedioximato, S = aromatic solvent).[3c,45] In the $Ni(dpg)_2I$, Ni(OMTBP)I, and $NiPcI_{1.0}$ structures, a column of metal-ligand moieties is surrounded by four parallel tunnels containing polyiodide molecules (I_5^- in the former, I_3^- in the latter cases). In contrast, a $M(bqd)_2$ column is surrounded by two tunnels containing polyiodide (I_3^-) and two containing solvent molecules.[5c] Viewed normal to the z axis the present structure consists of separate layers of iodide atoms and sheets of nickel complex separated by 1/4c; this is also the case for Ni(OMTBP)I and $Ni(bqd)_2I_{0.5}\cdot 1/2S$, but not for $Ni(dpg)_2I$. Successive phthalocyanine rings in the stack are staggered 39.5°, the closest intermolecular contacts in the stack being C(1)-C(1') and C(8)-C(8') at 3.252(2) and 3.258(2) Å, respectively. In the dimeric complex $(MnPyPc)_2O$,[27] the phthalocyanine rings are approximately parallel, separated by about 3.4 Å and staggered at 41°. In the phthalocyanine sandwich complexes of Sn[34] and U[35] the rings are much closer together (2.7-2.8 Å) and also staggered by about 40°. It was suggested that the yet unknown 45° staggered arrangement

would result in unfavorable contacts between α-pyrrole carbon atoms in $Sn(Pc)_2$.[34] In the present structure the 45° arrangement would not necessarily increase benzo-hydrogen atom contacts in the sheet, but it would decrease the C(1)-C(1') (and C(8)-C(8')) separations by 0.014 Å.

A most unusual feature of the present structure is the packing within the iodine chains. The observed I-I distance of 3.244(2) Å is nearly 1.0 Å shorter than twice the van der Waals' radius for I^- of 2.51 Å.[46] The thermal parameter along the chain direction is twice that perpendicular to the chain (Table III). We interpret these observations as indicating disorder of the iodine atoms and thus identify this as the cause of the diffuse scattering (see Experimental Section). The same conclusion was reached by Endres *et al.* for $Ni(bqd)I_{0.5}$.[5c]

The observed planes of diffuse intensity normal to the z axis imply one-dimensional order along z, and the spacing of the diffuse lines, $c^{*\prime} = 2/3c^*$, indicates that the repeat unit contains three Bragg sites. A reasonable model to account for this is the existence of ordered chains of I_3^- ions which are disordered with respect to their neighbors as shown in Figure 6. In each supercell two iodine atoms are displaced by an amount *d* from their average (Bragg) positions while one remains fixed, resulting in infinite chains of symmetric triiodide ions. Note that there are three distinct ways in which these chains can be ordered with respect to the arbitrary origin of the crystal. The intensity formula for this model[47] can be derived in a variety of ways; eq. (2) is obtained as a special case of a more general formula ($|F_d(\ell)|^2 = \langle FF^* \rangle - |\langle F \rangle|^2$) by Guinier, and is as follows:

$$|F_d(\ell)|^2 = (1/9)[(1+2\cos[2\pi\ell(d-1/3)])^2][9-(1+2\cos[2\pi\ell/3])^2] \qquad (2)$$

where ℓ refers to the supercell spacing c' = 3/2c. The general features of eq. (2) are such that the left-hand bracketed quantity vanishes for d = 0. (i.e., no disorder), and the right-hand quantity for ℓ = 3n (in agreement with experiment). It was the latter restriction which prevented the model in Figure 6 from being used for $Ni(bqd)_2I_{0.5}$, since there lines for ℓ = 3n were observed. A least-squares fit of the diffuse intensities to eq. (2) leads to a value of d of 0.0245(2). This corresponds to an I-I distance within the triiodide ion of 3.00 Å and I----I non-bonded contacts of 3.72 Å. Observed and calculated structure amplitudes are given in Table IX ; the final R index for the diffuse lines is 0.085. In view of the simplicity of the model, e.g., the explicit assumption of a symmetric I_3^- ion, the agreement is very satisfactory. It is doubtful that these limited data are amenable to analysis with a more complex model. The distances extracted from the diffuse intensity data are within the range 2.8 - 3.1 Å reported for triiodide ions[48,49] although bond distances >2.96 Å are ordinarily observed in asymmetric ions. The results support the existence of symmetrical I_3^- ions in NiPcI in complete agreement with the spectral data.

On the Nature of $NiPcI_x$ Stoichiometries where $x \neq 1$.

As noted earlier, powdered samples of $NiPcI_x$ can be prepared for a wide range of x. The resonance Raman and iodine Mössbauer results indicate that iodine is present predominantly if not exclusively as I_3^- up to $x \sim 3.0$. For $x \lesssim 1.0$, there is some evidence from the optical spectra that unoxidized NiPc may be present. However from such results it is not clear whether starting bulk NiPc or discrete NiPc molecules (or groups of molecules) integrated into a $NiPcI_x$ lattice are being observed. Indeed, the spectral

data provide no information on whether a single phase with a continuously varying iodine content or phases of discrete stoichiometries (or ranges of stoichiometries) might be present. This problem was investigated by X-ray powder diffractometry on $NiPcI_x$ samples where x = 0, 0.55, 1.0, 1.1, 2.64, and 4.01. Although the data were only evaluated in a semiquantitative fashion, the following conclusions could be reached. First, for $x < 1.0$, quantities of bulk, unoxidized NiPc were clearly present. The only other phase which could be detected was the x = 1.0 material. The presence of unoxidized NiPc is in accord with the optical spectra. Second, the materials with $x > 1$ contain no detectable NiPc. However in addition to varying amounts of the x = 1.0 material, they exhibit an additional phase with a new crystal structure, distinctly different from the x = 1.0 phase. No attempt was made to index this cell. Iodine oxidation of the related macrocycle Ni(OMTBP) has so far produced crystals with two stoichiometries, $x \approx 1$ and $x \approx 3$.[4a,d] The present powder diffraction results for $NiPcI_x$ suggest that there also may be only two phases with $x < 3$, one at x = 1, the other at $x \approx 3$.

$NiPcI_{1.0}$ Electron Resonance Spin g Values

$NiPcI_{1.0}$ crystals show a single moderately intense, rather narrow esr signal whose g-value and linewidth are angle dependent. The detailed study of the signal serves to identify the nature of the orbital which loses an electron upon partial oxidation of the NiPc. A combination of measurements of esr and static susceptibility give evidence regarding the interaction within a partially oxidized NiPc stack.

The g-tensor for $NiPcI_{1.0}$ crystals is axially symmetric with the needle (molecular normal) c axis corresponding to the unique $\parallel$ tensor axis. Figure 7 plots $g(\theta)$, the angle-dependent ambient temperature g-value for a repre-

sentative $NiPcI_{1.0}$ crystal, where θ is the angle between the magnetic field $\underline{H_0}$ and $\underline{c}$. The g-values can be fit to equation (3)

$$g(\theta) = [g_{\parallel}^2 \cos^2\theta + g_{\perp}^2 \sin^2\theta]^{1/2}, \qquad (3)$$

with $g_{\parallel} = 2.0075(2)$ and $g_{\perp} = 2.0007(2)$ for $NiPcI_{1.0}$. The observed angle dependence and the appreciable intensity of the signal unambiguously indicate that it represents the paramagnetic resonance of the hole-species produced by partial oxidation and not an impurity.

Both $g_{\parallel}$ and $g_{\perp}$ are very close to the free electron value of $g_e = 2.0023$. A metal-centered oxidation, however, would yield a hole species with the g-value of $[Ni^{III}Pc]^+$, far from g_e. The g-values for $[Ni^{III}Pc]^+$ have been found to be $g_{\perp} = 2.29$ and $g_{\parallel} = 2.11$.[50] The combination of nearly free electron g-values and narrow linewidths is characteristic of the phthalocyanine π-cation radical, $[Ni^{II}Pc^+]$, demonstrating that the oxidation is ligand-centered. Since partial oxidation involves removal of electrons from the highest occupied π-orbitals we may write with certainty the formula for the $NiPcI_{1.0}$ as $NiPc(I_3^-)_{0.33} = [Ni^{II}Pc]^{+0.33}(I_3)_{0.33}$.

A close inspection of the g-tensor, nevertheless, shows it to be anomalous. For either a π-cation radical or a planar Ni^{III} species, we expect $g_{\parallel} \sim g_e$ and $g_{\perp} > g_e$. However, for $NiPcI_{1.0}$, we find $g_{\parallel} > g_{\perp} \approx g_e$. The observed deviation $g_{\parallel} > g_e$ is precisely of the form expected for the contribution of a fractional hole density on the iodine chain. If we represent the structure by the basic unit of $(NiPc)_3^+I_3^-$, the simplest way to account

for spin density on iodine involves the inclusion of a small degree of back charge transfer. We schematically write a simple Mulliken charge transfer

$$|\psi\rangle = \sqrt{1-\alpha^2}\ |((NiPc)_3^+(I_3)^-\rangle + \quad (NiPc)_3(I_3)^\cdot\rangle \qquad (4)$$

wavefunction in which α^2 represents the degree of charge transferred from I_3^- back to the partially oxidized macrocycle. We show elsewhere that it is only possible to describe the results by assuming a ligand centered oxidation of NiPc, and derive the formula.[4d]

$$g_{\parallel} \approx g_e + 2\alpha^2 \qquad (5)$$

Employing the measured $g_{\parallel}$ gives $\alpha^2 \approx 0.002$ as the degree of back charge transfer from an I_3^- to the macrocyclic stack.

$NiPcI_{1.0}$ Electron Spin Resonance Linewidth

The esr lineshape, although roughly Lorentzian in character, is asymmetric. The degree of asymmetry is typically expressed as the ratio of the amplitude of the larger amplitude lobe of the derivative line, A, to that of the smaller lobe, B. For $NiPcI_{1.0}$ at room temperature, A/B = 1.40 ± 0.20.[51,52] This asymmetry is not due to the anomalous skin effect. First, the magnitude of the conductivity of $NiPcI_{1.0}$ at room temperature, although large, should not cause A/B to differ appreciably from unity and A/B does not increase when $\sigma_{\parallel}$ increases at low temperature. In addition, A/B is not a function of the angle (θ) between the needle c axis and the external field as seen in TSeF-TCNQ (TSeF = tetraselenafulvalene, and TCNQ = tetracyanoquinodimethane).[53] Because the asymmetry is small and independent of both

angle and temperature, further discussion of the linewidth will use the derivative peak-to-peak linewidth, Γ.

Figure 8 shows the angle dependence of the peak-to-peak linewidth. The variation with angle (Figure 8) can be approximately fit to the expression,[14]

$$\Gamma = \Gamma_0 + \Gamma_1 (1 + \cos^2\theta). \qquad (6)$$

with Γ_0 = 3.56 and Γ_1 = 1.76 gauss. Γ_1 is relatively constant from crystal to crystal. Γ_0 ranges between 1.5-4.0 gauss and is larger with crystals of larger cross sectional area. Thus there may be a contribution from crystal mosaicity. This angle dependence is the same as that observed for $Ni(OMTBP)I_{1.08}$.[4d] In this latter material the linewidth is found to be controlled by spin-lattice relaxation via polaron motion.[54] Even recognizing that the linewidth in $NiPcI_{1.0}$ is exchange or motionally narrowed, we note that the small residual value is characteristic of π-radicals, not of metal centered moments.

The temperature dependence of $\Gamma(\theta = 0,90)$ for $NiPcI_{1.0}$ is shown in Figure 9. The linewidth decreases slowly and approximately linearly with decreasing temperature down to 40-50 °K, where there is a noticeable flattening of the curve. No sharp changes in the spin susceptibility, χ^s, are observed in the region of the conductivity transition. Since the conductivity is metal-like in this region, the result suggests enhanced motional narrowing at lower temperature as carrier mobility is increasing. Alternatively, we note that in the Elliot linewidth mechanism, $\Gamma \alpha (\Delta g)^2 \tau^{-1}$,

where Δg is a measure of the g-anisotropy and τ is the scattering time.[55] Since $\sigma_{||}$ and thus τ increases at lower temperatures, for constant Δg, Γ is expected to decrease as T decreases, as is observed. Note that the linear dependence, $\Gamma \propto T$, and quadratic dependence, $\rho_{||} \propto T^2$ means that $\Gamma \propto \rho^{1/2}$.

NiPcI$_{1.0}$ Electron Spin Resonance Signal Intensity.

The room temperature esr intensity of NiPcI$_{1.0}$ was employed to determine that the spin susceptibility, χ^s, is $1.70 \pm 0.26 \times 10^{-4}$ emu/mole. The temperature dependence of the scaled esr integrated intensity, $I(T)/I(T_1)$, for a powder of NiPcI$_{1.0}$ is presented in Figure 10. The esr intensity remains essentially constant from room temperature until approximately 180 °K. Below aproximately 180 °K there is a gentle, roughly linear decrease until at 40 °K, the lowest temperature examined, the intensity is about half that at room temperature. The data for a single crystal, Figure 10, suggest a slightly stronger falloff, but the esr intensity from a single crystal is low, and in any case the differences in the measurements are not large.

The weak temperature dependence of the spin susceptibility and metal-like conductivity (vide infra) of NiPcI$_{1.0}$ at high temperatures (T > 180 °K) make it attractive to relate χ^s to the Pauli susceptibility of a degenerate electron gas. This permits an approximation of the intermolecular interaction within a stack of partially oxidized NiPc macrocycles in terms of t (the transfer integral) which is the one-electron matrix element for the inter-

molecular interaction. In a tight-binding band composed of the highest occupied molecular orbital on NiPc,

$$\chi^s = 2\beta^2 D(\epsilon(k_f)), \tag{7}$$

where χ^s is the energy, k_f is the Fermi level wavevector, and the one-dimensional density of states is given by,

$$D(\epsilon(k_f)) = \frac{N}{2\pi}(4t^2 - \epsilon(k)^2)^{-1/2} \tag{8}$$

with N the number of molecules per cubic centimeter.[2c] In $NiPcI_{1.0}$, the highest occupied band of doubly occupied states is partially emptied by ρ = 1/3 of an electron/molecule, leading to

$$k_f = (2 - \rho)\frac{\pi}{2\underline{a}} = 5\pi/6\underline{a}. \tag{9}$$

Thus the spin susceptibility for $NiPcI_{1.0}$ is

$$\chi^s = \beta^2 N/2\pi t \sin(5/6) \tag{10}$$

When equated to the experimental value of χ^s, this expression gives $t \sim 0.06$ eV and a bandwidth of $4t \sim 0.24$ eV. Although this model is an oversimplification, the value for t is of a reasonable magnitude for the overlappping ligand-centered π-orbitals. Similar values for t have been found for other molecular metals.[56] A bandwidth 0.20 eV is also found from thermoelectric power measurements and lends additional support for the application of one-dimensional tight-binding band theory to the properties of $NiPcI_{1.0}$.[57,58]

$NiPcI_{1.0}$ Static Magnetic Susceptibility

The measured static susceptibility at room temperature is $\chi^s = +3.40 \pm 0.21\ 10^{-6}$ emu/g, or $+2.32 \times 10^{-4}$ emu/mole. In order to obtain the diamagnetic correction, we have measured the susceptibility of NiPc, obtaining $\chi(NiPc) = -2.34 \times 10^{-4}$ emu/mole. Adding to this the Pascal's constant susceptibility for $(I + I + I^-)/3$[56b] as an approximation to the diamagnetism of 1/3 of I_3^-, we arrive at $\chi^d = -3.49 \pm 0.22 \times 10^{-4}$ emu/mole. The corrected paramagnetic susceptibility of $NiPcI_{1.0}$ is thus $\chi^P = 5.8 \pm 0.4 \times 10^{-4}$ emu/mole, equivalent to $\sim$2/3 electrons per site. This means that there is an excess paramagnetic contribution to the susceptibility, $\chi^P - \chi^s \approx 4.1 \times 10^{-4}$ emu/mole, beyond that observed by epr spectroscopy.

The static susceptibility is essentially constant down to 4°K.[60] Since the change in χ^s is just within the sensitivity limits of our static susceptibility measurement, this shows that the large excess susceptibility must be approximately temperature independent. We therefore equate this excess paramagnetic contribution with a van Vleck temperature independent paramagnetism, χ^v;[61] the following argument suggests that this is plausible.

The van Vleck susceptibility can be written[62]

$$\chi^v = \Sigma_i \frac{2n\beta^2\Lambda^2_i}{\Delta_i} \times \frac{MW(NiPcI_{1.0})}{\rho(NiPcI_{1.0})} \qquad (11)$$

where β is the Bohr magneton, n is the number of sites per cubic centimeter, $\Lambda_i = \langle i|L_z|0\rangle$ is the matrix element of the angular momentum operator, L_z, between the ground state of a molecule $|0\rangle$, and the i'th excited state $|i\rangle$, with excitation energy, $\Delta_i = E_i - E_0$. Equating the excess paramagnetic susceptibility at room temperature, 4.1×10^{-4} emu/mole, with the χ^v given

by equation 11 requires an excitation to be available at an energy of approximately

$$\Sigma_i \left(\frac{\Lambda^2_i}{\Delta_i}\right) = 6.3 \text{ eV}^{-1} \qquad (12)$$

The highest occupied and lowest unoccupied π-orbitals of phthalocyanine (and porphyrin) exhibit considerable orbital angular momentum with off diagonal matrix element L_z with $\Lambda = 3\text{-}6$;[63] the phthalocyanines also exhibit excited states starting at 1.77 eV (700 nm). Thus it seems likely that van Vleck paramagnetism can indeed account for the difference between the paramagnetic susceptibility measured by epr and the Faraday methods.

NiPcI$_x$ Electrical Conductivity.

The electrical conductivity of NiPcI$_x$ materials for a range of x values is surveyed in Table X. These data are for compressed polycrystalline samples and as such suffer from interparticle contact resistance effects and from being averaged over all crystallographic orientations (more informative single crystal results will be discussed shortly). Nevertheless, the powder conductivity data for a wide range of x are comparable with powder data for other "molecular metals", and experience with a variety of low-dimensional materials indicates that single crystal conductivities along the molecular stacking direction should be greater by a factor of 10^2-10^3. Variable temperature studies of electrical conductivity were carried out for several powder samples and thermally activated charge transport was observed. Apparent activation parameters could be obtained by least-squares fits to equation (13).

$$\sigma = \sigma_{\infty} e^{-E_a/kT} \qquad (13)$$

These parameters and standard deviations resulting from the fitting procedure are set out in Table X.

NiPcI$_{1.0}$ Single Crystal Conductivity.

Single crystals of NiPcI$_{1.0}$ are exceedingly thin and electrical conductivity could only be measured along the needle axis. At room temperature, the conductivity range for 65 samples was 260-750 $\Omega^{-1}cm^{-1}$, with an average value of 550 $\Omega^{-1}cm^{-1}$. These values are comparable with stacking axis conductivities of "organic metals" such as TTF-TCNQ (tetrathiafulvalene-tetracyanoquinodimethane).[2,64] However, because of the very large cross-sectional area of the phthalocyanine molecule, when comparing NiPcI$_{1.0}$ with other materials, it is instructive to consider the properties of the individual charge carriers. Within the framework of one-electron tight-binding band theory, the conductivity can be related to λ, the mean free path of a carrier along the stacking direction (the average distance between scattering events) and to a, the cross sectional area per conducting stack, by equation (14)

$$\sigma_{\parallel} = 4e^2\lambda/(ha) \qquad (14)$$

where e is the electronic charge and h is Planck's constant.[65] For NiPcI$_{1.0}$ we find λ to be in the range 3.3 to 8.2 Å or 1.0 to 2.3 intermolecular spacings. This result can be compared with the values for other highly conducting stacked molecular systems of 2.1 to 2.8 spacings for $(TTT)_2I_3$ (TTT = tetrathiatetracene),[66] 1-2 spacings for the related

metallomacrocycle Ni(tetrabenzporphyrin)I,[44] 1.6 to 2.5 spacings for HMTSF-TCN(HMTSF = hexamethylenetetraselenafulvalene),[67] 0.4 to 0.6 spacings for TTF-TCNQ,[68] 0.6 spacing for $K_2Pt(CN)_4Br_{0.3}\cdot 3H_2O$,[2c] and 0.04 spacing for the polaronic conductor Ni(octamethyltetrabenzoporphyrin)$I_{1.0}$.[56,54]

Figure 11 shows a plot of the temperature dependence of $NiPcI_{1.0}$ conductivity along the c axis. As the temperature is decreased below ambient, all $NiPcI_{1.0}$ crystals exhibit a rise in conductivity to a maximum at temperature T_m, and then an abrupt decrease. T_m is found to vary from crystal to crystal, and although typically about 100 °K, T_m values between approximately 180 °K and 55 °K were observed. Any crystal may be cycled repeatedly without hysteresis in $\sigma_{||}$ if T is maintained greater than T_m. Once cooled below T_m, however, most crystals never return to the initial room temperature value of $\sigma_{||}$ upon warming. Upon recooling, the discontinuity occurs at a higher temperature T_m', and at every temperature above T_m' the conductivity is less than had been measured on the initial cycle. Since contactless microwave measurements on $NiPcI_{1.0}$ show a reversible transition in $\sigma_{||}$ at the low end of our range of T_m values,[69] we conclude that in most instances the transition observed in the four-probe measurements is largely an artifact of stress on the crystal by the contact wires: the wires are typically of diameter comparable with a crystal.

Among the large number of $NiPcI_{1.0}$ crystals studied, and among those crystals showing the lowest T_m, one crystal (Figure 11) was seen to show a reversible "metal-semiconductor" transition for one cycle. The T_m value for this crystal is found to be ca. 52 °K, which is equal within the experimental error of the temperature measurement to the T_m found in the microwave measurements. Because this crystal was mounted using 0.0005 inch diameter

nickel wire, and was probably under much less strain than the majority of $NiPcI_{1.0}$ crystals, with some confidence we use the reversibility of the transition at T_m as the criterion to assign the value of ca. 52 °K as the true T_m for $NiPcI_{1.0}$. To provide further information on the nature of the 52 °K transition, resonance Raman spectra of $NiPcI_{1.0}$ crystals were recorded down to 8 °K. There was no change in the polyiodide scattering pattern which would indicate a change in the degree of charge transfer, i.e., appearance of an I_5^- or I_2 transition.

The analysis of the dependence of the $NiPcI_{1.0}$ conductivity in the region above T_m is not complicated by artifacts. All crystals cycled in the region T_m to 300°K show completely reversible behavior over three cycles, the maximum number performed. Thus for all crystals the data above T_m are taken as valid. Individual crystals show different $\sigma_{||}(T_1)$, (T_1 = 295 °K) and plots of $\sigma_{||}(T)/\sigma_{||}(T_1)$ are not overlapping. Figure 12 illustrates this behavior for four $NiPcI_{1.0}$ crystals. However, the temperature dependence of all crystals studied obeys the empirical relationship,[70]

$$\rho(T)/\rho(T_1) = a + b\,(T/T_1)^{\nu}, \qquad (15)$$

where a and b are constants, with a least-squares fit of the data yielding the result $\nu = 1.9 \pm 0.2$. The value of ν is different from unity found for simple metals and is reminiscent of that found for several other molecular metals, 2.0 to 2.4.[71] Crystals with the highest T_m give the poorest statistical fit to equation (15), probably because the data are obtained over a narrow range of temperature. In such cases the value of ν is not well determined and appears to vary from the value of 1.9 ± 0.2 exhibited by the

majority of crystals. A similar apparent dependence of on the temperature range of the data has been noted elsewhere.[70b]

From plots of $\sigma(T)/\sigma(T_1)$ versus temperature it is not obvious that a single conductivity mechanism applies to all crystals of a given material. The four $NiPcI_{1.0}$ data sets in Figure 12 are a good example. As an alternative mode of presenting the conductivity, a plot of the quantity $\ln-(1-[\rho(T)/\rho(T_1)])$ versus temperature may be employed.[72] As shown for the four representative $NiPcI_{1.0}$ crystals in Figure 12, this method yields a superimposable family of curves. The curves plotted in Figure 13 have not been overlapped in order that the behavior of each crystal may be easily observed. However, it is obvious that adjusting C for the lower three curves in Figure 13 would fully overlap them with the top curve. This result provides assurance of the reliability of the conductivity measurements and of a well defined scattering mechanism.

CONCLUSIONS

Partial oxidation of metallophthalocyanines with iodine has provided an extensive new class of molecular conductors. As illustrated in the present case with nickel phthalocyanine, the properties of the resulting solid state array of π-cation radicals include electrical conductivity which is comparable with that of the best-known stacked molecular conductors. A particularly intriguing feature of $NiPcI_{1.0}$ charge transport is a transition from metallic to semi-conducting behavior which apparently is not reflected in the magnetic properties of the carriers. It is tempting to speculate that this behavior reflects a change in carrier mobility brought about by some subtle structural rearrangement such as a change in the ordering of the triiodide chains. → next page

In a broader perspective, the iodinated metallophthalocyanines, such as those reported here, represent the first entry into a widening area of conductive materials based upon the ligand (π) systems of mixed-valent metallomacrocyclic arrays. Clearly the insights gleaned and the methodology developed will lead to an ever-deepening understanding of those molecular characteristics which facilitate charge conduction and which optimize materials performance.

ACKNOWLEDGMENTS

This research was generously supported by the NSF-MRL program through the Materials Research Center of Northwestern University (Grant DMR76-80847A01), by the NSF (Grant DMR77-26409 to BMH), and by the Office of Naval Research (to TJM). We thank Dr. Stanley L. Ruby of the Physics Division of Argonne National Laboratory for recording the iodine Mössbauer spectrum of $NiPc^{129}I_{2.16}$.

Supplementary Material. Table III, the root-mean-square amplitudes of vibration, and a listing of structure amplitudes (pages). Ordering information is given on any current masthead page.

References and Notes

(1) Camille and Henry Dreyfus Teacher-Scholar.

(2) (a) Miller, J.S.; Epstein, A.J., eds. Synthesis and Properties of Low-Dimensional Materials, Ann. N.Y. Acad. Sci., 1978, 313.
(b) Keller, H.J., ed. Chemistry and Physics of One Dimensional Metals, Plenum Press, New York, 1977.
(c) Miller, J.S.; Epstein, A.J. Prog. Inorg. Chem., 1976, 20, 1-151.
(d) Keller, H.J., ed. Low Dimensional Cooperative Phenomena, Plenum Press, N.Y., 1975.

(3) (a) Petersen, J.L.; Schramm, C.S.; Stojakovic, D.R.; Hoffman, B.M.; Marks, T.J. J. Am. Chem. Soc., 1977, 99, 286-288.
(b) Schramm, C.S.; Stojakovic, D.R.; Hoffman, B.M.; Marks, T.J. Science, 1978, 200, 47-48.

(4) (a) Phillips, T.E.; Hoffman, B.M. J. Am. Chem. Soc., 1977, 99, 7734-7736.
(b) Hoffman, B.M.; Phillips, T.E.; Schramm, C.J.; Wright, S.K., p. 393-398 in "Molecular Metals", W.E. Hatfield, ed., Plenum Press (1979).
(c) Wright, S.K.; Schramm, C.J., Phillips, T.E.; Scholler, D.M.; Hoffman, B.M. (1979/80) Synthetic Metals 1, 43-51.
(d) Phillips, T.E.; Scaringe, R.P.; Hoffman, B.M.; Ibers, J.A. J. Am. Chem. Soc., 1980, in press.

(5) (a) Marks, T.J. in reference 2a, p. 594-616.
(b) Cowie, M.; Gleizes, A.; Grynkewich, G.W.; Kalina, D.W.; McClure, M.S.; Scaringe, R.P.; Teitelbaum, R.C.; Ruby, S.L.; Ibers, J.A.; Kannewurf, C.R.; Marks, T.J. J. Am. Chem. Soc., 1979, 101, 2921-2936.
(c) Brown, L.D.; Kalina, D.W.; McClure, M.S.; Ruby, S.L.; Schultz, S.; Ibers, J.A.; Kannewurf, C.R.; Marks, T.J. J. Am. Chem. Soc., 1979, 101, 2937-2947.

(6) (a) Scaringe, R.P.; Ibers, J.A. Acta Crystallogr., 1979, A35, 803-810.
(b) Megtert, S.; Pouget, J.P.; Comès, R. in reference 2a, p. 234-243.
(c) Endres, H.; Keller, H.J.; Mégnamisi-Bélombé, M.; Moroni, W.; Pritzkow, H.; Weiss, J.; Comes, R. Acta Crystallogr., 1976, A32, 954-957.

(7) Corfield, P.W.R.; Doedens, R.J.; Ibers, J.A., Inorg. Chem., 1967, 6, 197-204.

(8) The Northwestern absorption program, AGNOST, includes both the Coppens-Leiserowitz-Rabinosvich logic for Gaussian integration and the Tompa analytical method. In addition to various local programs for the CDC-6100 computer, modified versions of the following programs were employed; Zalkin's FORDAP Fourier summation program, Johnson's ORTEP thermal ellipsoid plotting program, and Busing's and Levy's ORFFE error function program. Our full-matrix, least-squares program, NUCLS, in its non-group form closely resembles the Busing-Levy ORFLS program. The diffractometer was run under the disk-oriented Vanderbilt system (P.G. Lenhert, J. Appl. Cryst., 1975, 8, 568-570).

(9) Azaroff, L. V. Acta Crystallogr., 1955, 8, 701-704.

(10) Supplementary material.

(11) (a) Teitelbaum, R.C.; Ruby, S.L.; Marks, T.J. J. Am. Chem. Soc., 1979, 101, 7568-7573.
(b) Teitelbaum, R.C.; Ruby, S.L.; Marks, T.J. J. Am. Chem. Soc., in press.

(12) (a) Ruby, S. L. Mössbauer Effect Methodology, 1973, 8, 263-276.
(b) The traditional goodness-of-fit parameter

$$\chi^2 = \sum_i^n [(\chi_i - \chi_{ic})/\Delta_{\chi_i}]^2$$

gives satisfactorily small values for either a good model (the calculated values χ_{ic} agree well with the data χ_i) or for a poor experiment ($\chi\Delta_i$ is large).

(13) Shenoy, G.K.; Friedt, J. M.; Maletta, H.; Ruby, S. L. Mossbauer Effect Methodology , 1974, 9, 277-305.

(14) Wertz, J.E.; Bolton, J.R. "Electron Spin Resonance", McGraw-Hill Book Company, New York, N.Y., 1972.

(15) Duffy, Jr., W.; Strandburg, D.L., J. Chem. Phys., 1967, 46, 456-

(16) (a) Seeger, K. Semiconductor Physics, Springer-Verlag, N.Y., 1973, p. 483-487.
(b) Cahen, D.; Anderson, J.R. Rev. Sci. Instrum., 1973, 44, 1567-1568.

(17) Phillips, T.E.; Anderson, J.R.; Schramm, C.J.; Hoffman, B.M. Rev. Sci. Instrum., 1979, 50, 263-265.

(18) (a) Teitelbaum, R.C.; Ruby, S.L.; Marks, T.J. J. Am. Chem. Soc., 1978, 100, 3215-3217.
(b) Marks, T.J.; Webster, D.F.; Ruby, S.L.; Schultz, S. J. Chem. Soc. Chem. Comm., 1976, 444-445.
(c) Kalina, D.W.; Stojakovic, D.R.; Teitelbaum, R.C.; Marks, T.J., manuscript in preparation.

(19) (a) Warshel, A. Ann. Rev. Biophys. Bioeng., 1977, 6, 273-300, and references therein.
(b) Spiro, T.J. in "Chemical and Biochemical Applications of Lasers," Moore, C.B., ed., Academic Press, N.Y ., Vol. 1, 1974, p. 29-70, and references therein.

(20) (a) Woodruff, W.H.; Pastor, R.W.; Dabrowiak, J.C. J. Am. Chem. Soc., 1976, 98, 7999-8006.
(b) Nafie, L.A.; Pastor, R.W.; Dabrowiak, J.C.; Woodruff, W.H. J. Am. Chem. Soc., 1976, 98, 8007-8014.
(c) Clark, R.J. H.; Turtle, P.C.; Strommen, D.P.; Streusand, B.; Kincaid, J.; Nakamoto, K. Inorg. Chem., 1977, 16, 84-89.
(d) Streusand, B.; Kowal, A.T.; Strommen, D.P.; Nakamoto, K. J. Inorg. Nucl. Chem., 1977, 39, 1767-1771.

(21) Lin, L.-S.; Wang, T.-C.; McClure, M.S.; Kannewurf, C.R.; Marks, T.J., submitted for publication.

(22) Reddy, J.M.; Knox, K.; Robin, M.B. J. Chem. Phys, 1964, 40, 1082-1089.

(23) (a) Marks, T.J.; Stojakovic, D.R. J. Am. Chem. Soc., 1978, 100, 1695-1705, and references therein.
(b) Schaffer, A.M.; Gouterman, M.; Davidson, E.R. Theor. Chim. Acta, 1973, 30, 9-30.
(c) Edwards, L.; Gouterman, M. J. Mol. Spectrosc., 1970, 33, 292-310.

(24) Day, P.; Scregg, G.; Williams, R.J.P. J. Chem. Phys., 1963, 38, 2778-2779.

(25) Potasek, M.J.; Debrunner, P.G.; Morrison, W.H., Jr.; Hendrickson, D.N. J. Chem. Phys., 1974, 60, 2203-2206.

(26) (a) Gibb, T.C. Principles of Mossbauer Spectroscopy, Chapman and Hall, London, 1976, Chapt. 4.2.
(b) Bancroft, G.M.; Platt, R.H. Adv. Inorg. Chem. Radiochem., 1972, 15, 59-258.

(27) Vogt, Jr., L.H.; Zalkin, A.; Templeton, D.H. Inorg. Chem, 1967, 6, 1725-1730.

(28) Brown, C. J. J. Chem. Soc. (A), 1968, 2488-2493.

(29) Brown, C. J. J. Chem. Soc. (A), 1968, 2494-2498.

(30) Hoskins, B.F.; Mason, S.A.; White, J.C.B. Chem. Comm., 1969, 554-555.

(31) Ukei, K. Acta Crystallogr., 1973, B29, 2290-2292.

(32) Fischer, M.S.; Templeton, D.H.; Zalkin, A.; Calvin, M. J. Am. Chem. Soc., 1971, 93, 2622-2628.

(33) Friedel, M.K.; Hoskins, B.F.; Martin, R.L.; Mason, S.A. Chem. Comm., 1970, 400-401.

(34) Bennett, W.E.; Broberg, D.E.; Baenziger, N.C. Inorg. Chem., 1973, 12, 930-936.

(35) Gieren, A.; Hoppe, W. Chem. Commun., 1971, 413-414.

(36) Rogers, D.; Osborn, R.S. Chem. Commun., 1971, 840-841.

(37) Kirner, J.F.; Dow, W.; Scheidt, W.R. Inorg. Chem., 1976, 15, 1685-1690.

(38) Scheidt, W.R.; Dow, W. J. Am. Chem. Soc., 1977, 99, 1101-1104.

(39) For a short compilation of such distances see ref. 37, Table XII.

(40) Hoard, J.L.; Hamor, M.J.; Hamor, T.A.; Caughey, W.S. J. Am. Chem. Soc., 1965, 87, 2312-2319.

(41) For an extensive tabulation see Day, V.W.; Marks, T.J.; Wachter, W.A. J. Am. Chem. Soc., 1975, 97, 4519-4527, Table VII.

(42) Hoard, J.L. in "Porphyrins and Metalloporphyrins", Smith, K.M. ed., American Elsevier Publishing Company, New York, N.Y., 10017, 1975, pp. 328-335.

(43) Christensen, A.T.; Thom, E. Acta Crystallogr., 1971, B27, 581-586.

(44) Phillips, T. E.; Pace, L.; Hoffman, B. M.; Ibers, J. A., manuscript in preparation.

(45) Endres, H.; Keller, H.J.; Moroni, W.; Weiss, J. Acta Crystallogr., 1975, B31, 2357-2358.

(46) Pauling, L. "The Nature of the Chemical Bond", 3rd ed., Cornell Univ. Press, Ithaca, New York, 1960.

(47) Guinier, A."X-Ray Diffraction in Crystals, Imperfect Crystals and Amorphous Bodies", (W. H. Freeman and Co., San Francisco, 1963), p. 165.

(48) Popov, A.I. in "Halogen Chemistry", Vol. 1, Gutmann, V., ed., Academic Press, New York, N.Y., 1967, p. 225.

(49) Runsink, J.; Swen-Walstra, S.; Migchelsen, T. Acta Crystallogr., 1972, B28, 1331-1335.

(50) Bobrovskii, A. P.; Sidorov, A. N. J. Struct. Chem.(Eng.), 1976,, 17, 50-54.

(51) Feher, G.; Kip, A. F.; Phys. Rev., 1955, 98, 337-348.

(52) Dyson, F. J. Phys. Rev., 1955, 98, 349-359.

(53) (a) Tomkiewicz, Y.; Engler, E. M.; Schultz, T. D. Phys. Rev. Lett., 1975, 35, 456-459.
(b) Etemad, S.; Engler, E. M.; Schultz, T. D.; Penney, T.; Scott, B.A. Phys. Rev. B, 1978, 17, 513-528.

(54) Phillips, T. E.; Hoffman, B. M.; Soos, Z. G. Solid State Comm., in press.

(55) Elliott, R. J. Phys. Rev., 1954, 96, 266-279.

(56) Torrance, J. B.; Tomkiewicz, Y.; Silverman, B. D. Phys. Rev. B, 1977, 15, 4738-4749.

(57) Unpublished results of R.L. Green, IBM Research, San Jose, Calif. The measured thermoelectric power for $NiPcI_{1.0}$ was s = +20 μV/°K.

(58) An alternative interpretation of the magnetic behavior might be considered. The temperature dependence of the spin susceptibility is also similar to that predicted theoretically for a one-dimensional antiferromagnetic Heisenberg chain.[59] This model predicts the relationship between the temperature, T_s, at which χ^s peaks and the coupling between

$$kT_s = 1.282\ |J|,$$

spins, J, where k is Boltzmann's constant.[59] Interpretation of the susceptibility of $NiPcI_{1.0}$ with this model requires $J \gtrsim 140$ °K. The spin susceptibility at T = 0 °K in this model is given by the equation,

$$\chi_0^s = 2N\beta^2 b/\pi^2 J$$

where N is Avogadro's number, β is the Bohr magneton, and b is the degree of band filling.[56] For $NiPcI_{1.0}$, b = 5/6. The value of χ_0^s predicted for our value of J for $NiPcI_{1.0}$ is 4.52×10^{-4} emu/mole. This is more than double the value $\chi_0^s \sim 2 \times 10^{-4}$ emu/mole expected if the susceptibility maximum comes near to room temperature and far exceeds the estimate of 8.5×10^{-5} emu/mole, obtained by extrapolating the data of Figure 10 to 0 °K. Thus the Hubbard model does not appear to be applicable to the $NiPcI_{1.0}$ system.

(59) DeJongh, L.J.; Miedema, H.R. Adv. Phys., 1974, 23, 1-260.

(60) Unpublished results of A. Thompson, Exxon Research, Linden, N. J. on samples of $NiPcI_{1.7}$.

(61) J.H. Van Vleck, "The Theory of Electric and Magnetic Susceptibilities", Oxford University Press, London, 1932.

(62) C. Kittel, "Introduction to Solid State Physics", J. Wiley and Sons, Inc., New York, N. Y., 1971.

(63) Canters, G.W.; Van Egmond, S.; Schaafsma, T.J.; Chan, I.Y.; Van Drop, W.G.; Van der Waals, J.H. Ann. New York Acad. Sci., 1973, 206, 711-721.

(64) (a) Devreese, J.T.; Evrard, V.E.; Van Doren, V.E., eds, Highly Conducting One-Dimensional Solids, Plenum Press, N. Y. 1979.
(b) Torrance, J.B. Accts. Chem. Res., 1979, 12, 79-86.

(65) (a) Berlinsky, A. J. Contemp. Phys., 1976, 17, 331-354.
(b) Mott, N. F.; Davis, E. A. "Electronic Processes in Noncrystalline Materials", Clarendon Press, Oxford, 1971.

(66) Isett, L.C.; Perez-Albuerne, E. A. Solid St. Commun., 1977, 21, 433-435.

(67) (a) Bloch, A. N.; Cowan, D. O.; Bechgaard, K.; Pyle, R. E.; Banks, R.H.; Poehler, T.O. Phys. Rev. Lett., 1975, 34, 1561-1564.
(b) Greene, R. L.; Mayerle, J. J.; Schumaker, R.; Castro, G.; Chaikin, P. M.; Etemad, S.; LaPlaca, S. J. Solid State Commun., 1976, 20, 943-946.

(68) Etemad, S.; Engler, E. M.; Schultz, T.D.; Penney, T.; Scott, B.A. Phys. Rev. B, 1978, 17, 513-528.

(69) Poehler, T.; private communication.

(70) (a) Seiden, P.E.; Cabib, D. Phys. Rev. B, 1976, 13, 1846-1849.
(b) Chiang, C.K.; Cohen, M.H.; Newman, P.R.; Heeger, A.J. Phys. Rev. B , 1977, 16, 5163-5172.

(71) Andre, J.J.; Bieber, A.; Gautier, F. Ann. Phys., 1976, 1, 145-256.

(72) Groff, R.P.; Suna, A.; Merrifield, R.E. Phys. Rev. Lett., 1974, 33, 418-421.

Table I. Reaction Conditions[a] and Analytical Data for $NiPcI_x$ Samples

x	Weight (mmole) NiPc, g	Weight (mmole) I_2, g	Volume Solvent,[a] ml.	Elemental Analysis, Calcd. (Found) C	H	N	I
0.30	0.71 (1.24)	b	50	63.07 (63.89)	2.63 (2.58)	18.40 (19.16)	6.26 (6.37)
0.58	0.30 (0.53)	0.056 (0.22)	5	59.83 (58.68)	2.49 (2.40)	17.43 (17.71)	11.08 (11.06)
1.07	0.30 (0.53)	0.11 (0.43)	5	54.34 (54.77)	2.26 (2.20)	15.85 (15.58)	
1.44	0.30 (0.53)	0.16 (0.63)	5	50.96 (51.00)	2.12 (2.49)	14.86 (14.69)	
2.79	0.56 (0.92)	b	100	41.51 (42.48)	1.73 (1.79)	12.11 (12.51)	38.30 (39.36)
3.81	0.34 (0.60)	b	100	36.41 (36.60)	1.52 (1.75)	10.62 (10.45)	

[a]See Experimental Section for procedures.

[b]A saturated solution of iodine in chlorobenzene was employed.

Table II. Crystal Data and Experimental Details

Compound	Ni(phthalocyanine)I
Formula	$NiC_{32}H_{16}N_8I$
Formula Weight	698.15 amu
Cell: a	18.936(6) Å
c	6.488(3) Å
V	1260.1 Å^3
Z	2
Density: calc.	1.84 g/cm^3
obs.	1.78(4) g/cm^3
Space Group	D_{4h}^2-P4/mcc
Crystal Shape	Needle of octagonal cross section bounded by faces of the forms {100}, {110}, and {001} with separations of 0.040, 0.042, and 0.712 mm, respectively.
Radiation	Cu $K\alpha_1$
	111.4 cm^{-1}
Transmission Coefficients	0.499-0.713
Take-off Angle	3.5°
Receiving Aperture	5.8 mm high x 5.0 mm wide 26 cm from crystal
Receiving Counter	34 cm from crystal
Scan Speed	2°/min
Scan Width	0.85° below $K\alpha_1$ to 0.9° above $K\alpha_2$ for $2.0 \leq 2\theta \leq 90.0°$

Table II Continued.

	1.0 below $K\alpha_1$ to 1.0 above $K\alpha_2$ for $90.0 \leq 2\theta \leq 125.0°$
	1.5 below $K\alpha_1$ to 1.0 above $K\alpha_2$ for $125.0 \leq 2\theta \leq 160.0°$
Background Counts	40 sec total for singly scanned peaks
Data Collected	$h \geq k \geq 0 \pm \ell$ $2\theta < 90°$ $h \geq k \geq 0 + \ell$ $90° < 2\theta < 160°$
Unique Data (after averaging Friedel pairs)	630
Unique Data with $F_o^2 > 3\sigma(F_o^2)$	375
R for last cycle of refinement	0.042
R_w on F_o	0.051
R Final cycle of F_o^2	0.058 ($F_o^2 > 3\sigma(F_o^2)$)
R_w	0.113
Final Number of Variables	65

Table III. Positional and Thermal Parameters for the Atoms of NiPcI

ATOM	X[A]	Y	Z	B_{11} OR B_{11}[B]	B_{22}	B_{33}	B_{12}	B_{13}	B_{23}
I	1/2	1/2	1/4	6.02(5)	6.02	56.88(52)	0	0	0
NI	0	0	0	3.84(8)	3.84	14.92(52)	0	0	0
N(1)	0.12241(48)	0.05788(39)	0	4.43(36)	3.19(31)	14.3(14)	0.28(28)	0	0
N(2)	0.08299(42)	0.22879(43)	0	4.25(39)	4.56(39)	16.1(15)	-0.18(32)	0	0
C(1)	0.14278(51)	0.15335(47)	0	4.58(47)	3.88(41)	11.5(14)	-0.43(38)	0	0
C(2)	0.24543(51)	0.17133(51)	0	3.79(48)	5.84(46)	16.1(17)	-0.66(35)	0	0
C(3)	0.30856(50)	0.25379(56)	0	4.17(50)	4.67(47)	21.8(20)	-0.22(40)	0	0
C(4)	0.40801(62)	0.24464(63)	0	5.25(51)	6.01(55)	34.8(28)	-1.66(45)	0	0
C(5)	0.44165(60)	0.15366(66)	0	4.29(48)	6.94(61)	36.8(28)	-1.17(44)	0	0
C(6)	0.38723(54)	0.07871(59)	0	4.73(49)	5.12(50)	28.8(23)	0.82(38)	0	0
C(7)	0.28706(52)	0.08869(55)	0	3.98(42)	5.53(52)	15.5(18)	0.15(36)	0	0
C(8)	0.21809(49)	0.01864(61)	0	3.58(39)	5.37(50)	12.8(19)	-0.57(37)	0	0
H1 C(3	0.271	0.318	0	4.8					
H1 C(4	0.448	0.301	0	5.9					
H1 C(5	0.512	0.158	0	5.6					
H1 C(6	0.417	0.887	0	4.8					

[A] ESTIMATED STANDARD DEVIATIONS IN THE LEAST SIGNIFICANT FIGURE(S) ARE GIVEN IN PARENTHESES IN THIS AND ALL SUBSEQUENT TABLES. [B] THE FORM OF THE ANISOTROPIC THERMAL ELLIPSOID IS: $\exp(-(B_{11}H^2 + B_{22}K^2 + B_{33}L^2 + 2B_{12}HK + 2B_{13}HL + 2B_{23}KL))$. THE QUANTITIES GIVEN IN THE TABLE ARE THE THERMAL COEFFICIENTS $\times 10^3$.

Table IV. Root-Mean-Square Amplitudes of Vibration (Å) for NiPcI

Atom	Min.	Inter.	Max.
I	0.243(1)	0.243(1)	0.346(2)
Ni	0.178(3)	0.195(2)	0.195(2)
N(1)	0.175(9)	0.176(9)	0.210(9)
N(2)	0.185(9)	0.204(10)	0.212(9)
C(1)	0.158(9)	0.169(11)	0.213(11)
C(2)	0.185(10)	0.186(10)	0.229(10)
C(3)	0.214(11)	0.215(10)	0.247(10)
C(4)	0.197(12)	0.269(12)	0.269(11)
C(5)	0.195(12)	0.270(12)	0.277(11)
C(6)	0.216(11)	0.225(11)	0.244(10)
C(7)	0.182(10)	0.196(11)	0.234(11)
C(8)	0.160(10)	0.181(10)	0.233(11)

Table V. Resonance Raman Vibrational Data[a] for $NiPcI_x$ Compounds[b]

x	$\nu_{I_3^-}$, cm^{-1}	Other, cm^{-1}	Range recorded, cm^{-1}
0.00		592s, 687s, 1140m, 1340s, 1554vs, 1607m	60-2000
0.30	107s, 214m, 322m, 429w	172w	60-500
0.58	107vs, 214m		60-250
1.00[c]	107vs, 214s, 372m, 429m	92vw, 121w	60-500
1.44	107s, 214m		60-250
1.56	107s, 214m, 322w, 429vw	172vw	60-500
1.68	107vs, 214s, 322m, 429w, 535vw	172w, 587w, 685w, 1136w, 1340vw, 1550w, 1606m, 1858m	50-2000
2.79	107vs, 215s, 320m, 426w	172m	30-500
3.81	107s, 215m, 320w	179m, 291vw	60-350

[a] ν_o = 5145 Å.
[b] s = strong; m = medium, w = weak, sh = shoulder, v = very.
[c] Crystals over the temperature range 8-455 °K.

Table VI. Iodine-129 Mössbauer Parameters for $NiPc^{129}I_{2.16}$[a]

Parameter	Site 1	Site 2
δ, mm/sec[b]	1.34(5)	0.27(5)
e^2qQ, MHz[c]	-1667(10)	-862(10)
relative population	1.0	1.7(2)
Misfit[d]	3.4%	

[a]At 4 °K.
[b]Vs. ZnTe.
[c]For ^{129}I.
[d]Defined in Experimental section.

Table VII. Observed Distances and Angles in NiPcI

Atoms	Distance (Å)	Atoms	Angle (deg.)
Ni-N(1)	1.887(6)	N(1)-Ni-N(1')	90.00
N(1)-C(1)	1.370(8)	C(1)-N(1)-C(8)	106.3(6)
N(1)-C(8)	1.387(8)	C(1)-N(2)-C(8)'	119.2(6)
N(2)-C(1)	1.313(8)	N(2)-C(1)-N(1)	128.7(7)
N(2)-C(8')	1.326(9)	N(2)-C(1)-C(2)	119.8(6)
C(1)-C(2)	1.451(9)	N(1)-C(1)-C(2)	111.6(6)
C(2)-C(3)	1.382(10)	C(3)-C(2)-C(7)	121.1(6)
C(2)-C(7)	1.392(10)	C(3)-C(2)-C(1)	133.4(7)
C(3)-C(4)	1.392(10)	C(7)-C(2)-C(1)	105.5(6)
C(4)-C(5)	1.394(11)	C(2)-C(3)-C(4)	118.5(7)
C(5)-C(6)	1.383(10)	C(3)-C(4)-C(5)	119.8(8)
C(6)-C(7)	1.392(10)	C(6)-C(5)-C(4)	122.1(8)
C(7)-C(8)	1.461(9)	C(5)-C(6)-C(7)	117.4(8)
		C(2)-C(7)-C(6)	121.0(7)
		C(2)-C(7)-C(8)	106.9(7)
		C(6)-C(7)-C(8)	132.1(8)
		N(2)-C(8)-N(1)	128.4(6)
		N(2)-C(8)-C(7)	121.9(6)
		N(1)-C(8)-C(7)	109.6(7)
		Ni-N(1)-C(1)	127.2(5)
		Ni-N(1)-C(8)	126.4(5)

Table VIII. Comparison of Bond Parameters in NiPcI with Those in MgPc, ZnPc, FePc, and MnPc.

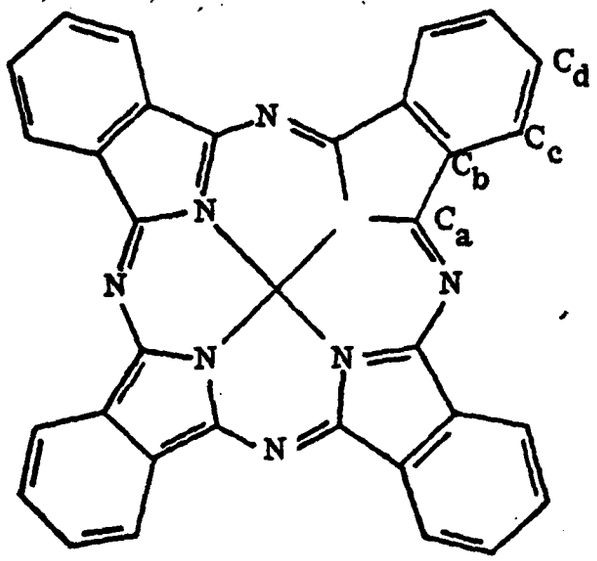

Bond Parameter [a,b]	NiPcI		Mean[c]	
N_p-C_a	1.379(12)		1.376(10)	
N_m-C_a	1.320(9)		1.328(7)	
C_a-C_b	1.456(7)		1.453(3)	
C_b-C_b	1.392(10)	1.389(6)	1.395(4)	1.392(6)
C_d-C_d	1.394(11)		1.394(2)	
C_b-C_c	1.387(7)		1.394(2)	
C_c-C_d	1.388(6)		1.385(7)	
C_a-N_p-C_a	106.3(6)		108.1(8)	
N_p-C_a-C_b	110.6(14)		109.3(4)	
C_a-C_b-C_b	106.2(10)		106.7(3)	
C_a-C_b-C_c	132.8(9)		132.2(2)	
C_b-C_c-C_d	118.0(8)		117.3(2)	
C_b-C_b-C_c	121.05(7)	121.0(9)	121.3(2)	121.4(2)
C_d-C_d-C_c	121.0(16)		121.6(1)	

Table VIII Continued.

Bond Parameter	NiPcI	Mean[c]
N_p-C_a-N_m	128.6(2)	127.7(1)
C_a-N_m-C_d	119.2(6)	123.2(5)

[a] N_p = pyrrole nitrogen, N_m = azamethine nitrogen.

[b] Numbers in parenthesis are deviations in the mean if averaging was possible.

[c] These are the average values from MgPc,[32] ZnPc,[38] FePc,[37] and MnPc.[37]

Table IX. Observed and Calculated Structure Amplitudes for Diffuse Lines in NiPcI.

ℓ'	$\lvert F_o \rvert$	$\lvert F_c \rvert$
1	19.4	14.4
2	25.3	23.0
4	43.7	46.0
5	33.3	31.7
7	55.7	53.9
8	20.4	21.8
10	42.3	44.0
11	4.5	8.1

$R = 0.081$

Table X. Conductivity Data for Polycrystalline Samples of Various $NiPcI_x$ Materials[a]

Compound	x	Room temperature conductivity, $\Omega^{-1}cm^{-1}$	Activation energy for conductivity, eV[b]
$NiPcI_x$	0	1×10^{-11}	1.6
	0.56	0.7	0.024
	0.58	2.2	
	1.0	0.7	0.036
	1.07	7.7	
	1.44	7.7	
	1.68	0.8	0.021
	3.81	0.6	

[a]Pressed pellets studied by four-probe van der Pauw technique (see Experimental Section).
[b]From least-squares fit to eq. (13).

Figure Legends

Figure 1. Resonance Raman spectra (ν_0 = 5145Å) of solid samples of: A, $NiPcI_{1.0}$; B, $NiPcI_{3.81}$.

Figure 2. Electronic absorption spectra (Nujol mulls) of solid samples of: A, $NiPcI_{1.0}$; B, $(benzamide)_2H^+I_3^-$; C, NiPc.

Figure 3. Iodine-129 Mössbauer spectrum of $NiPcI_{2.16}$. The solid line represents the optimized fit to the data points shown.

Figure 4. Stereo view of the crystal packing for $NiPcI_{1.0}$. Hydrogen atoms are shown as circles of arbitrary diameter.

Figure 5. Perspective view of the NiPc macrocycle, hydrogen atoms omitted.

Figure 6. Disorder model for the iodine chains in $NiPcI_{1.0}$. Average positions are shown as x's, the three distinct supercells each containing three such sites are shown with the same scale on the right.

Figure 7. Angular dependence of the g-value for the esr signal of $NiPcI_{1.0}$. The orientation $\theta = 0$ is such that the principal crystal axis is parallel to H_0.

Figure 8. Angular dependence of the esr linewidth at room temperature for $NiPcI_{1.0}$. Included (solid line) is the calculated dependence from the experimental data to eq. 6 (see text).

Figure 9. Temperature dependence of the esr linewidth, $H_0 \parallel \underline{c}$ (o) and $H_0 \perp \underline{c}$ (●), for $NiPcI_{1.0}$.

Figure 10. Temperature dependence of the intensity of the esr signal of $NiPcI_{1.0}$. Powder (●). Single crystal (△), H_0 $\underline{c}$. All values are given relative to the intensity at 297 °K.

Figure 11. Temperature dependence of the conductivity for a $NiPcI_{1.0}$ crystal showing totally reversible behavior down to 25 °K.

Figure 12. Temperature dependence of the conductivity ratio $\sigma_{\perp}(T)/\sigma_{\perp}(297K)$ of four $NiPcI_{1.0}$ crystals at temperatures above their individual conductivity maxima.

Figure 13. Plot of $\ln [1.0-\rho(T)/\rho(297K)]$ versus temperature for the four $NiPcI_{1.0}$ crystals of Figure 12.

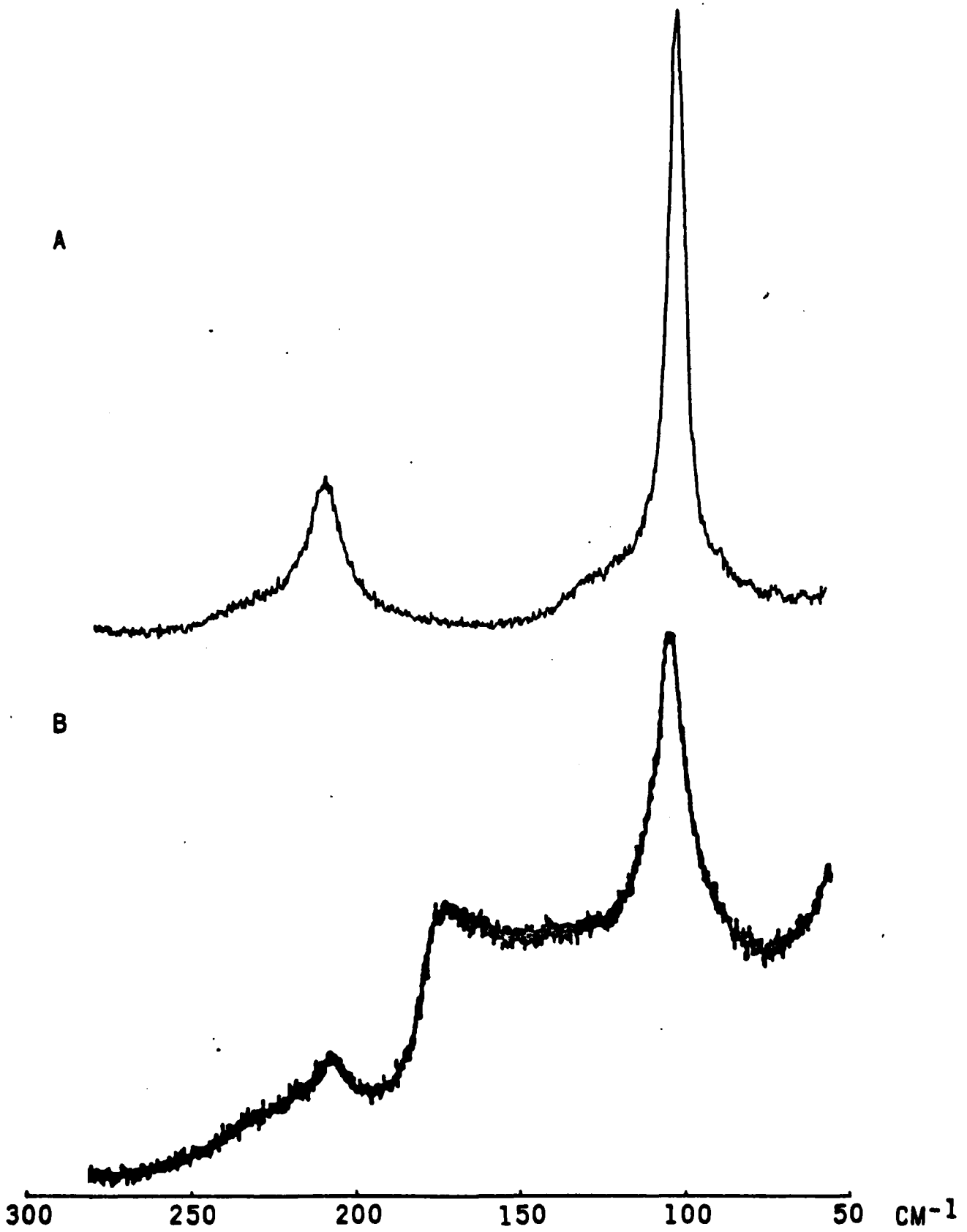
A
B
300
250
200
150
100
50
CM-1

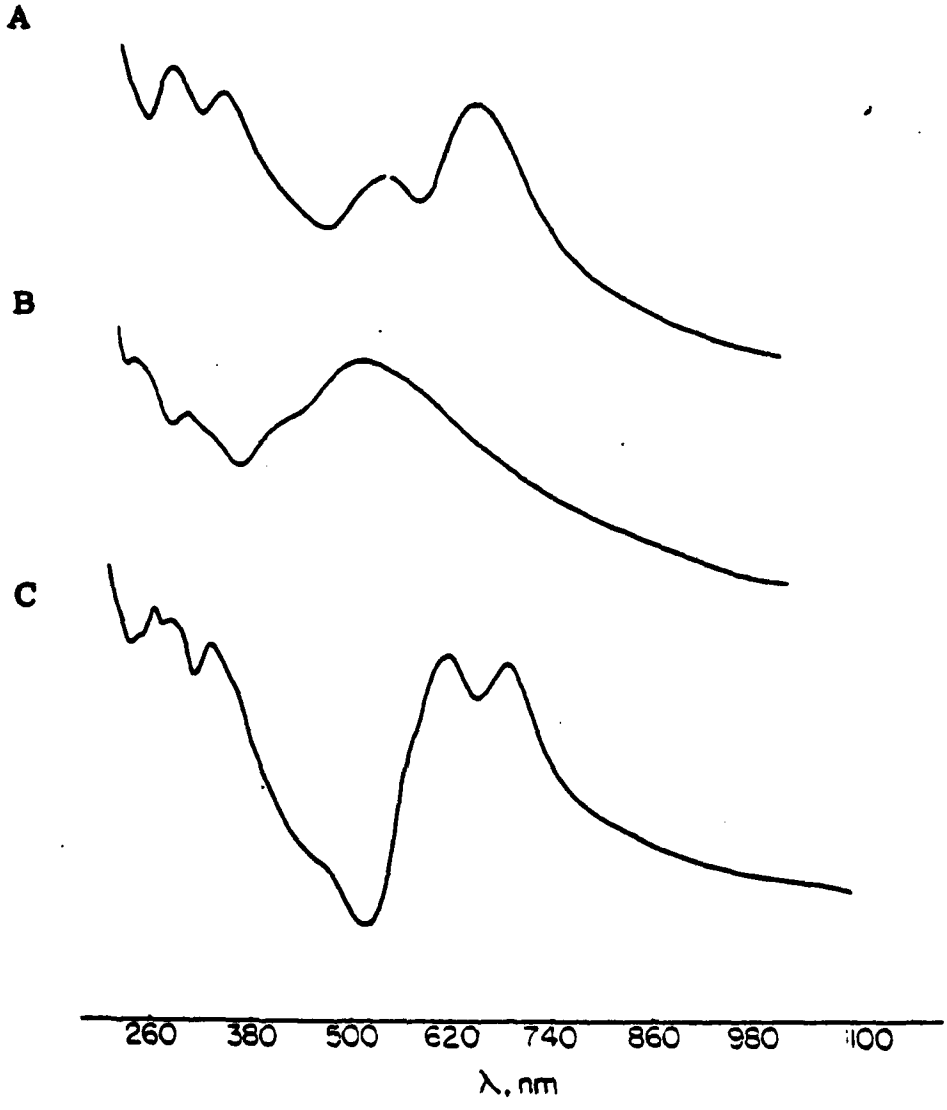
A
B
C
260
380
500
620
740
860
980
100
λ, nm

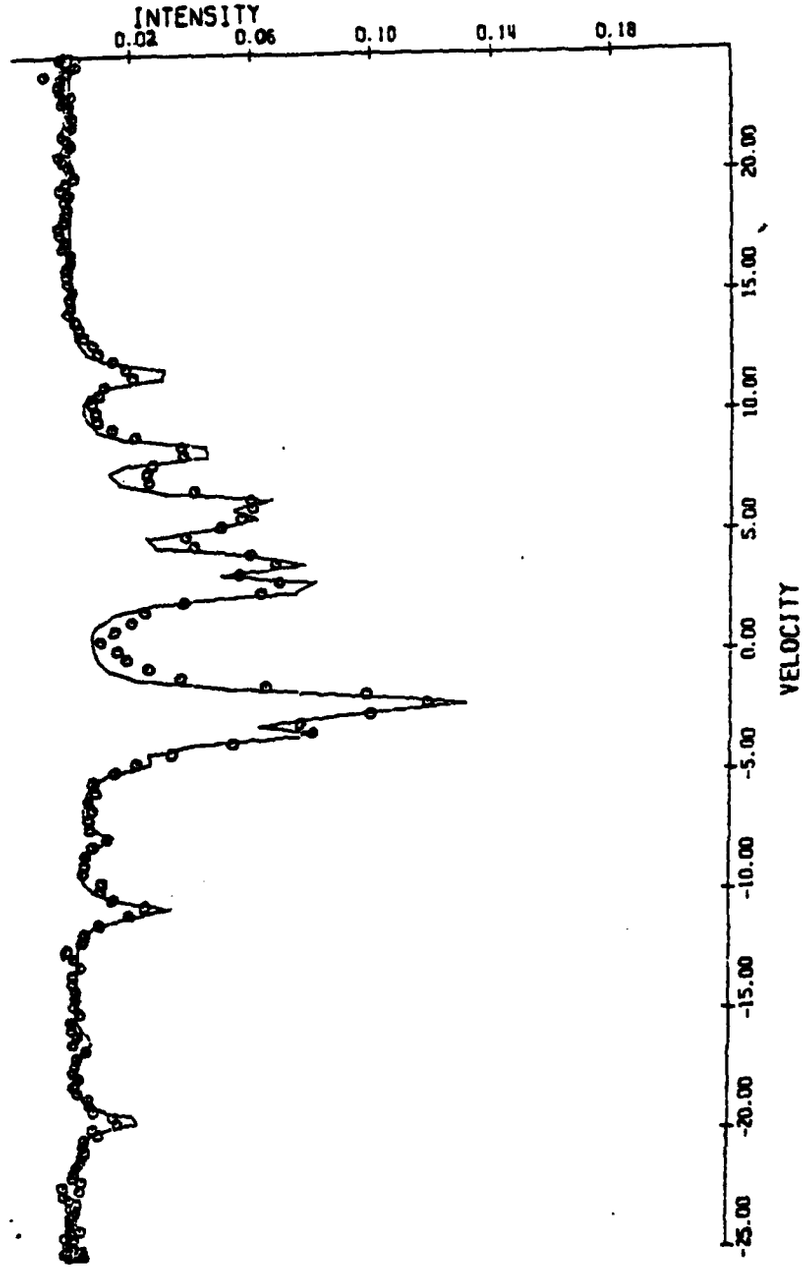
INTENSITY
0.02
0.06
0.10
0.14
0.18
20.00
15.00
10.00
5.00
0.00
-5.00
-10.00
-15.00
-20.00
-25.00
VELOCITY

TOP ACTUAL SIZE

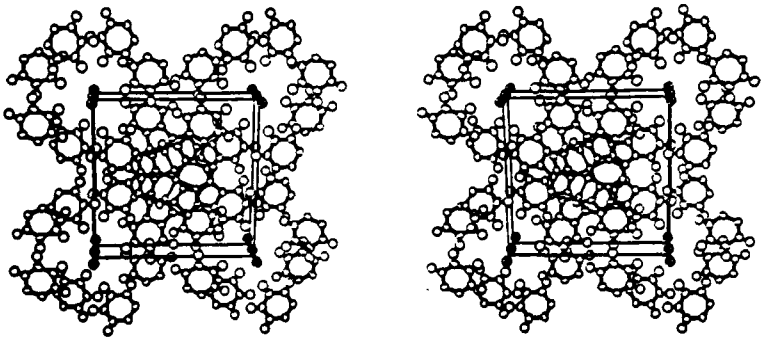

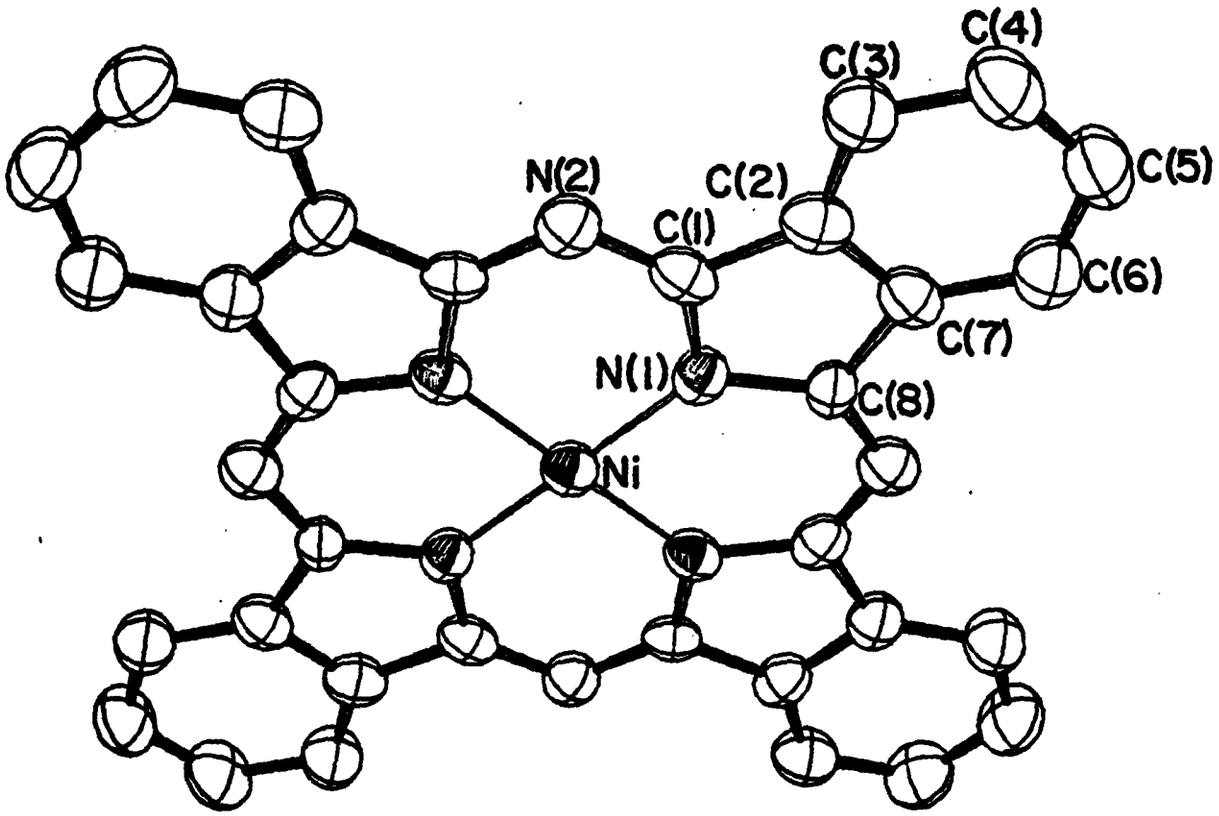
C(4)
C(3)
C(5)
N(2)
C(2)
C(1)
C(6)
C(7)
N(1)
C(8)
Ni

DISORDERED TRIIODIDE IONS IN Ni(Pc)I

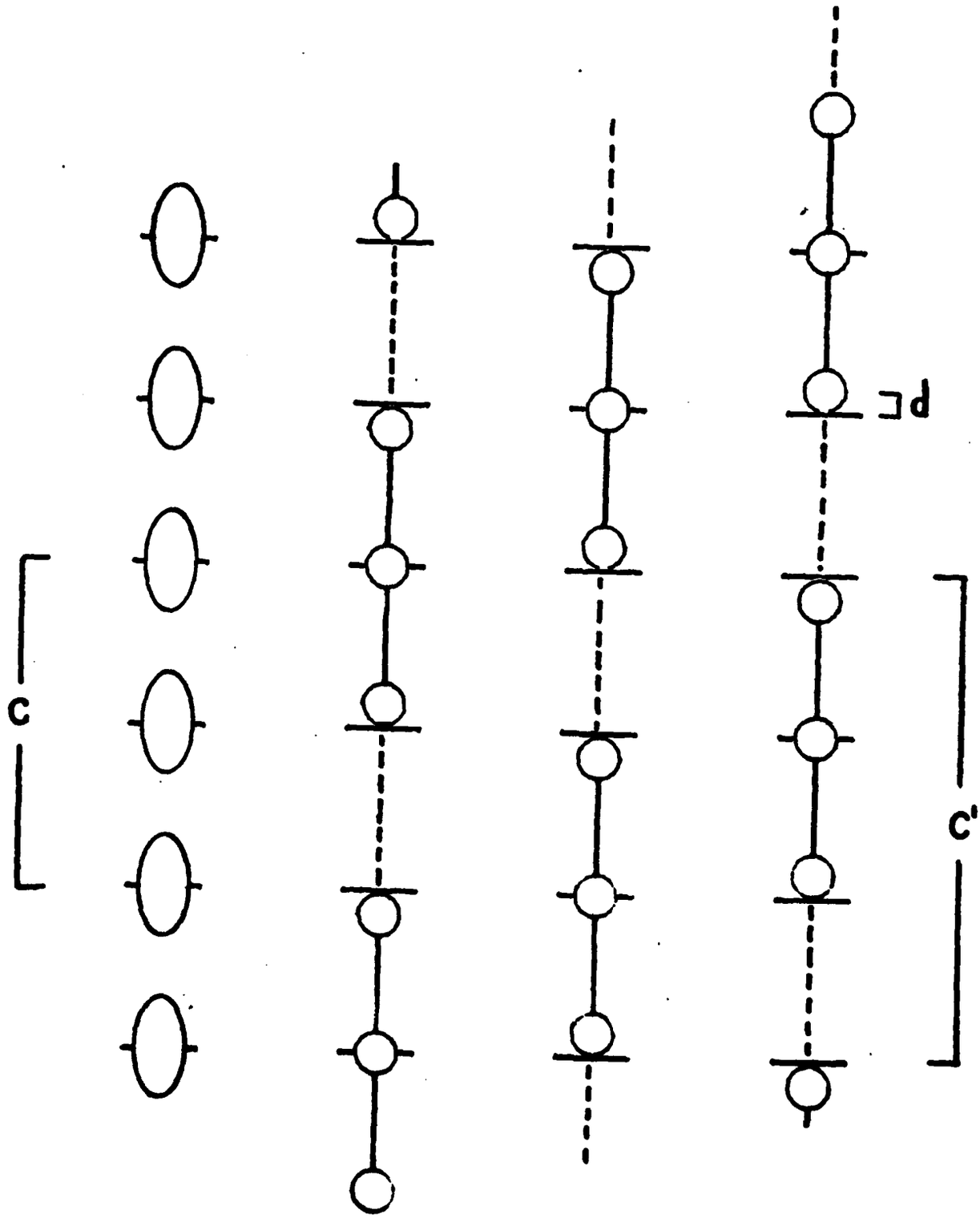

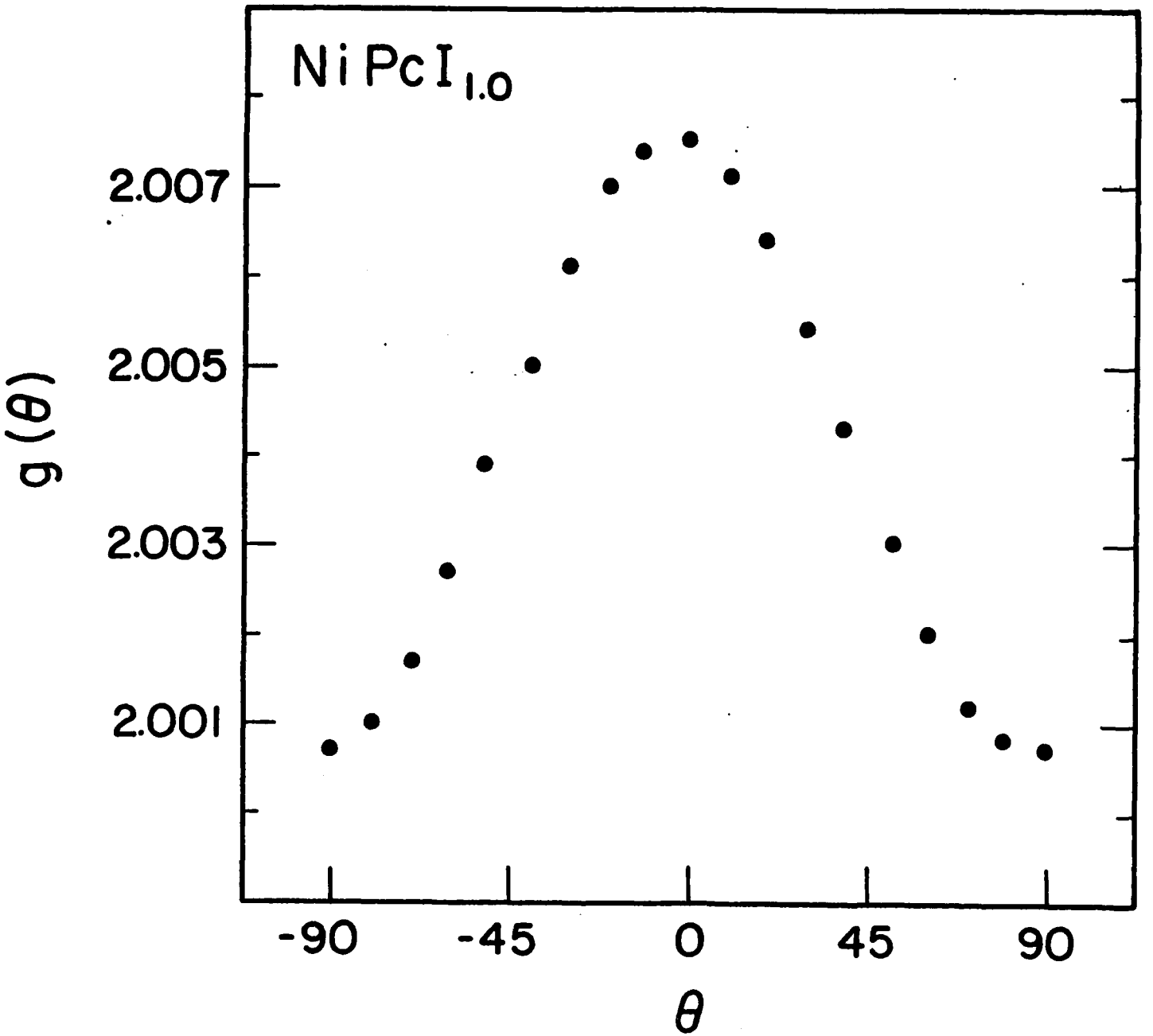
NiPcI1.0
2.007
2.005
2.003
2.001
g(θ)
-90
-45
0
45
90
θ

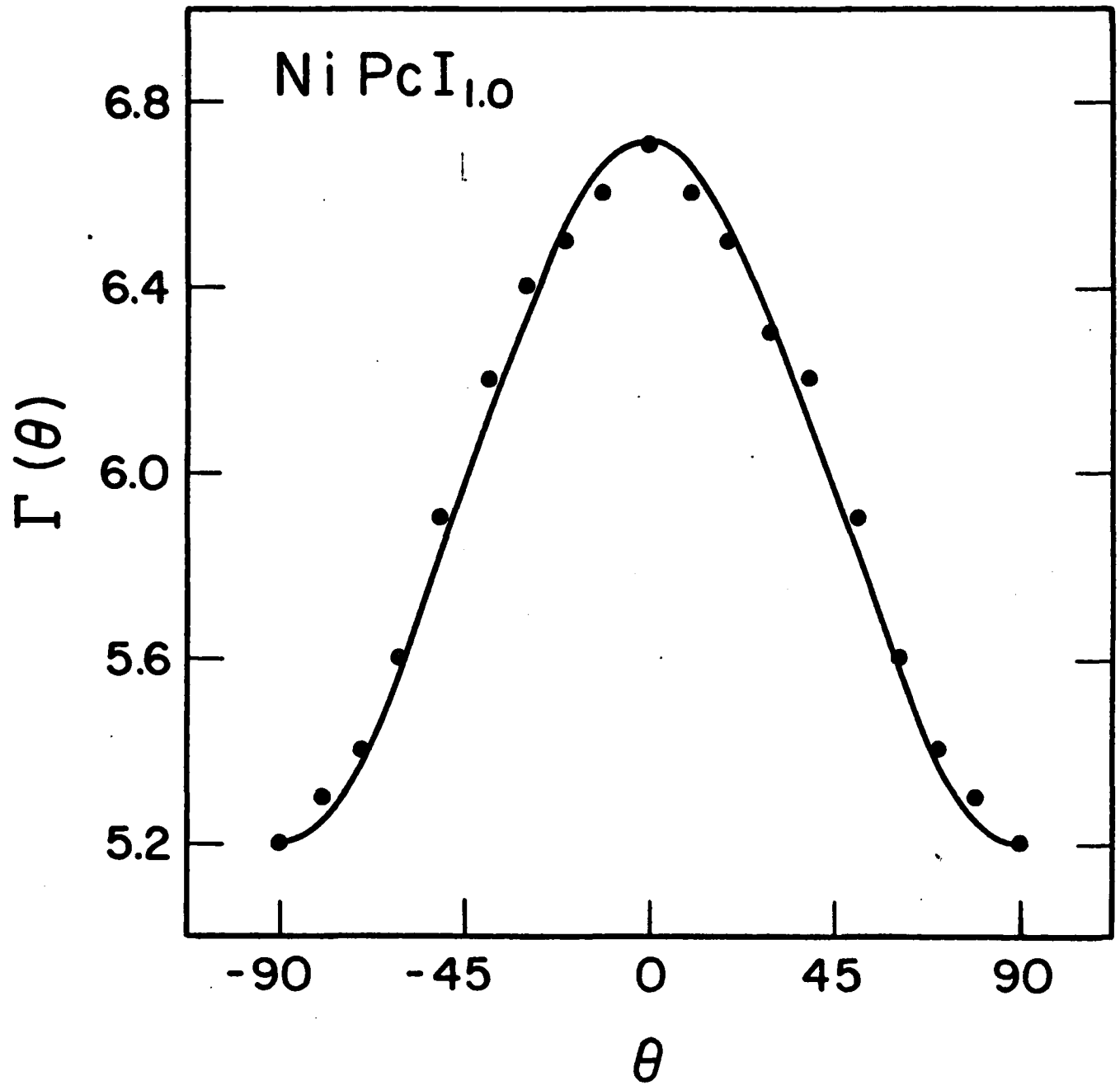
NiPcI1.0
6.8
6.4
6.0
5.6
5.2
Γ(θ)
-90
-45
0
45
90
θ

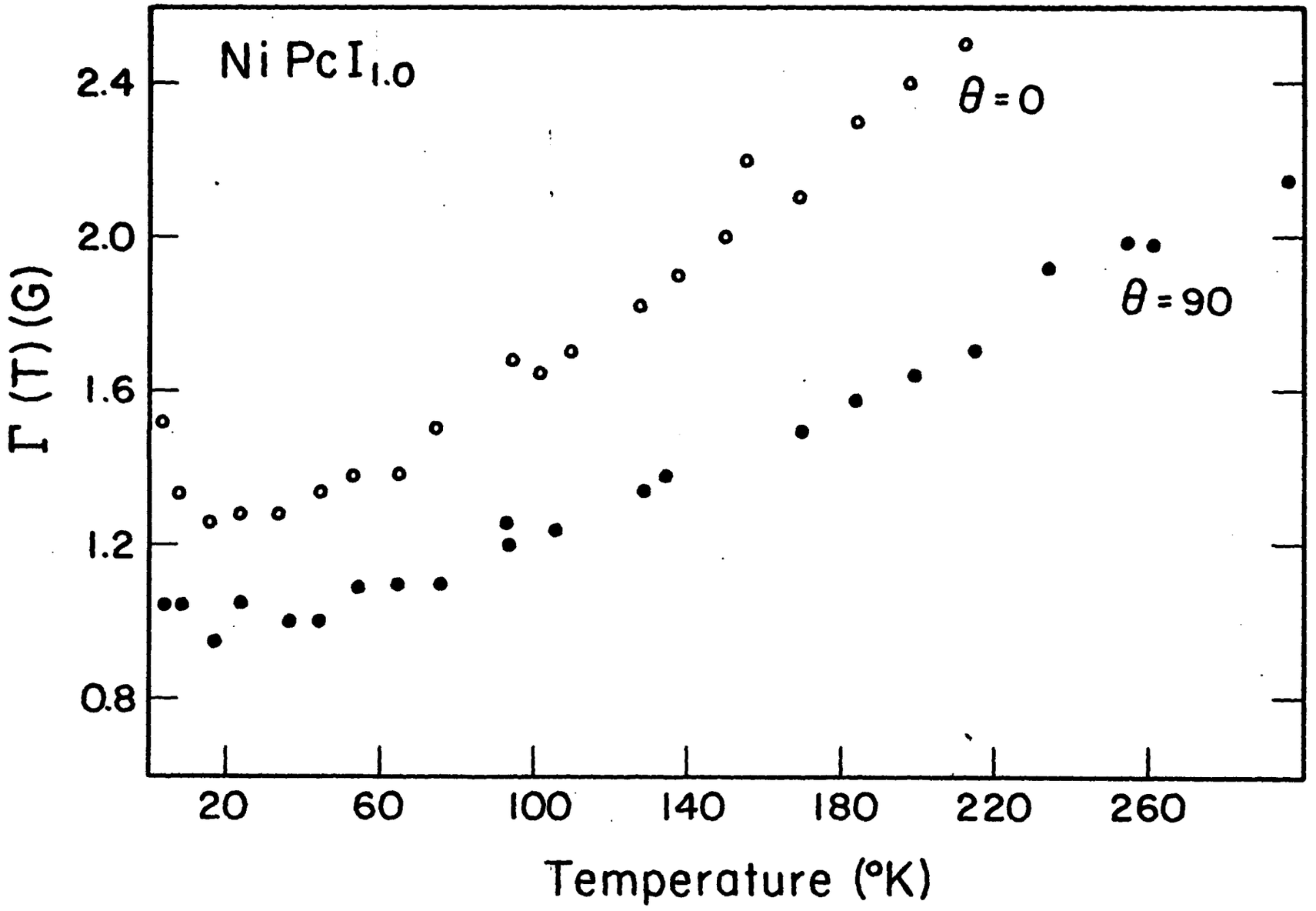
NiPcI1.0
θ=0
θ=90
Γ (T) (G)
2.4
2.0
1.6
1.2
0.8
20
60
100
140
180
220
260
Temperature (°K)

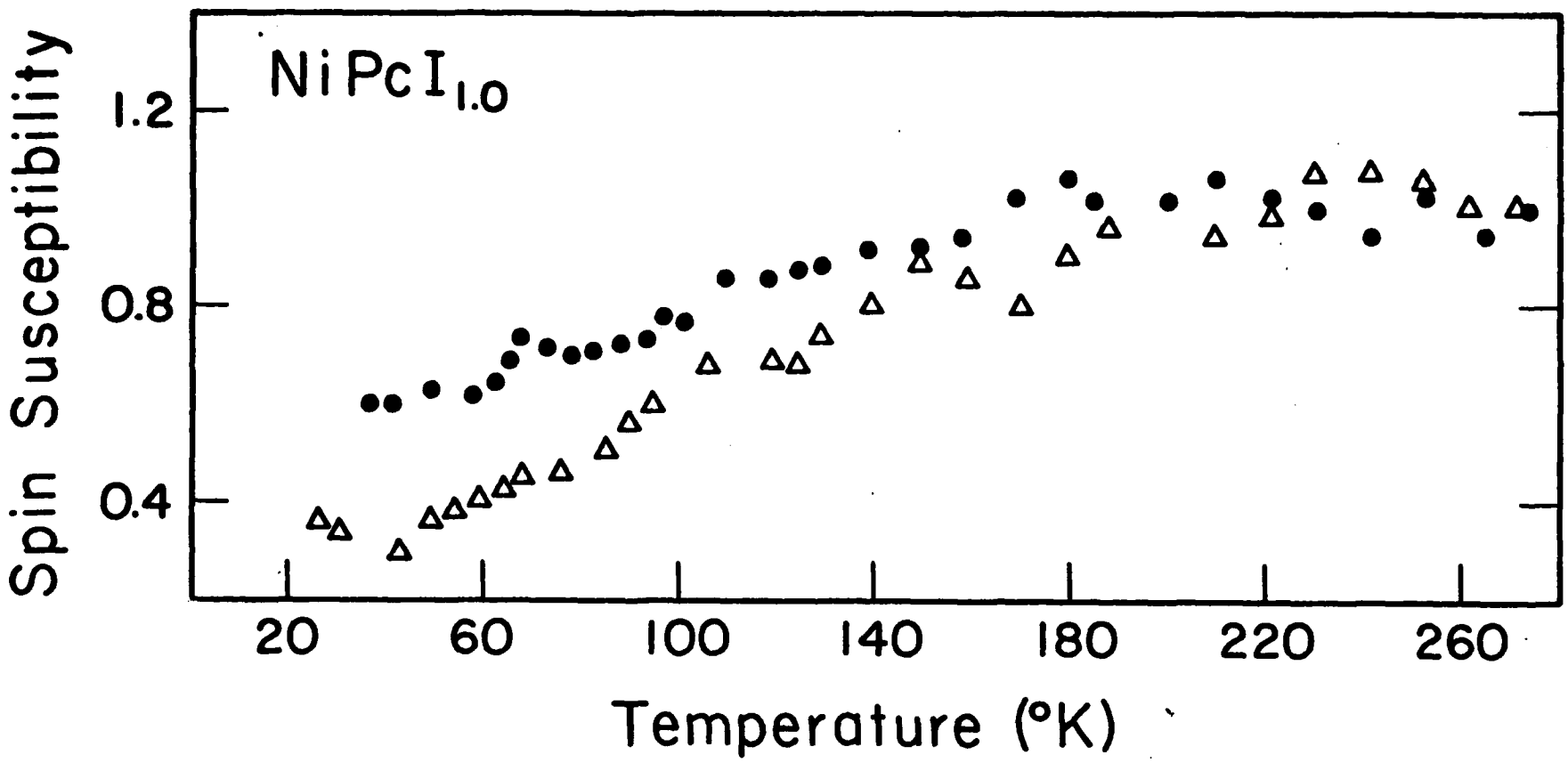
NiPcI1.0
Spin Susceptibility
1.2
0.8
0.4
20
60
100
140
180
220
260
Temperature (°K)

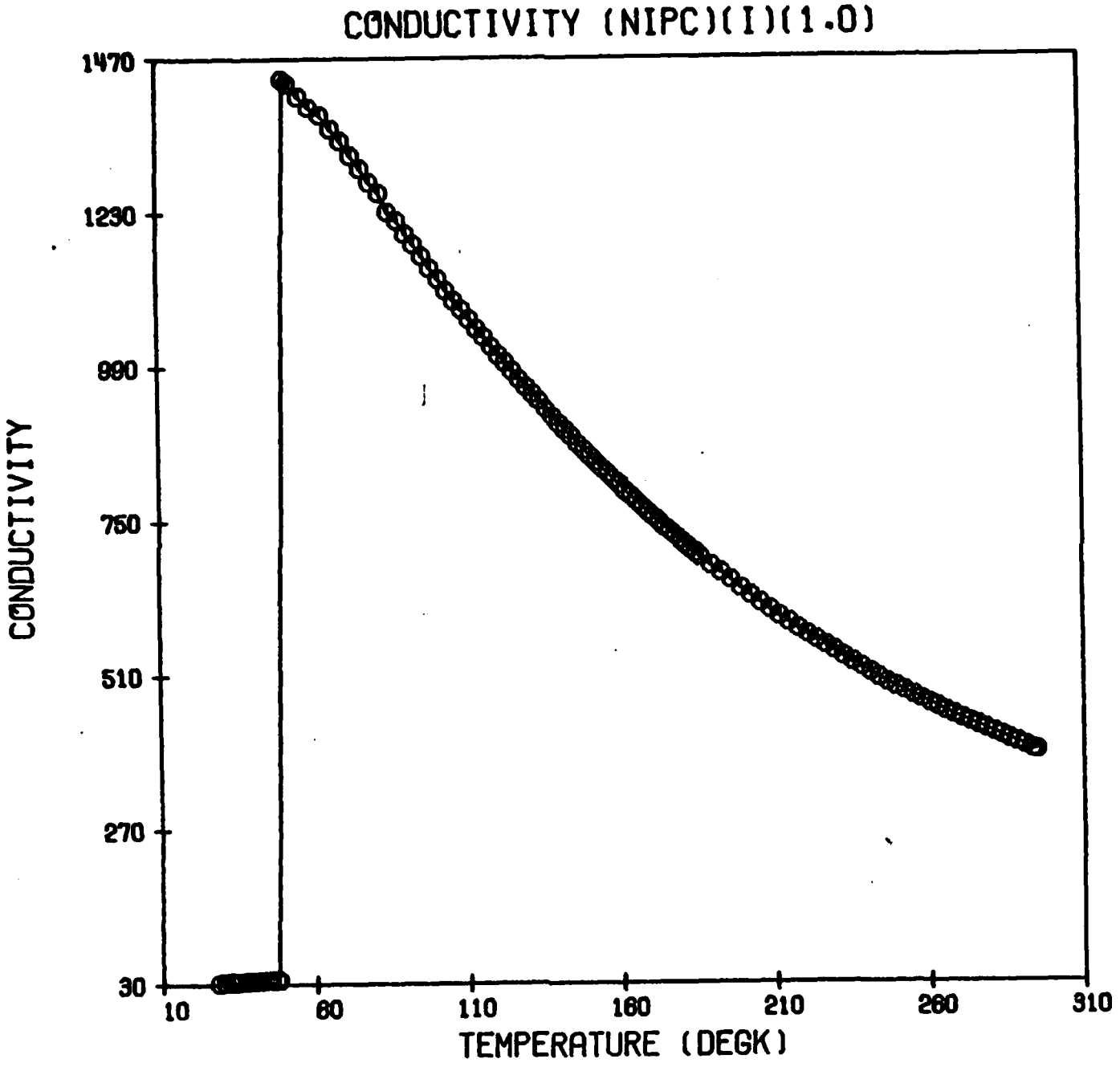
CONDUCTIVITY (NIPC)(I)(1.0)
1470
1230
990
750
510
270
30
CONDUCTIVITY
10
60
110
160
210
260
310
TEMPERATURE (DEGK)

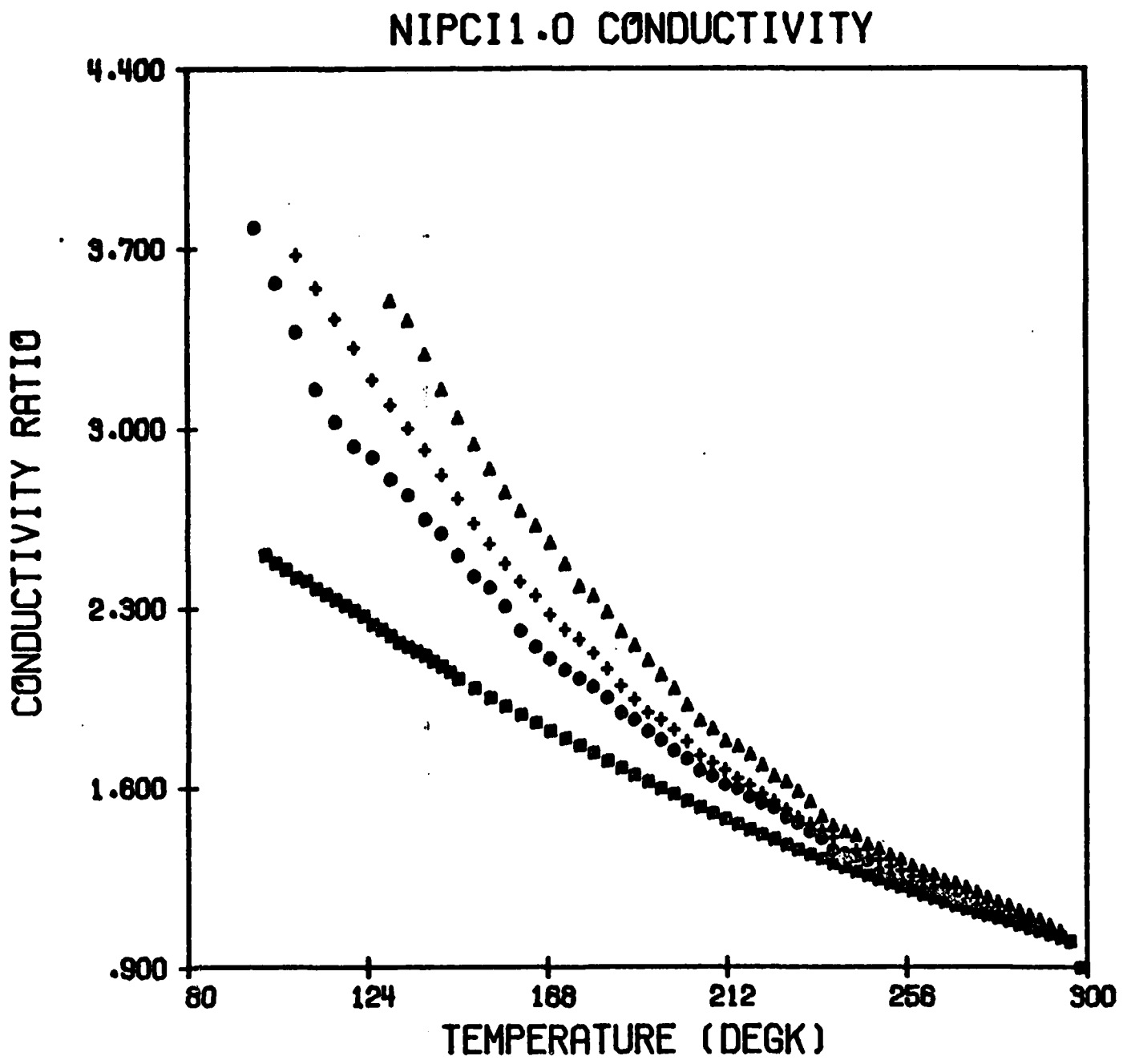
NIPCI1.0 CONDUCTIVITY
4.400
3.700
3.000
2.300
1.600
.900
CONDUCTIVITY RATIO
80
124
168
212
256
300
TEMPERATURE (DEGK)

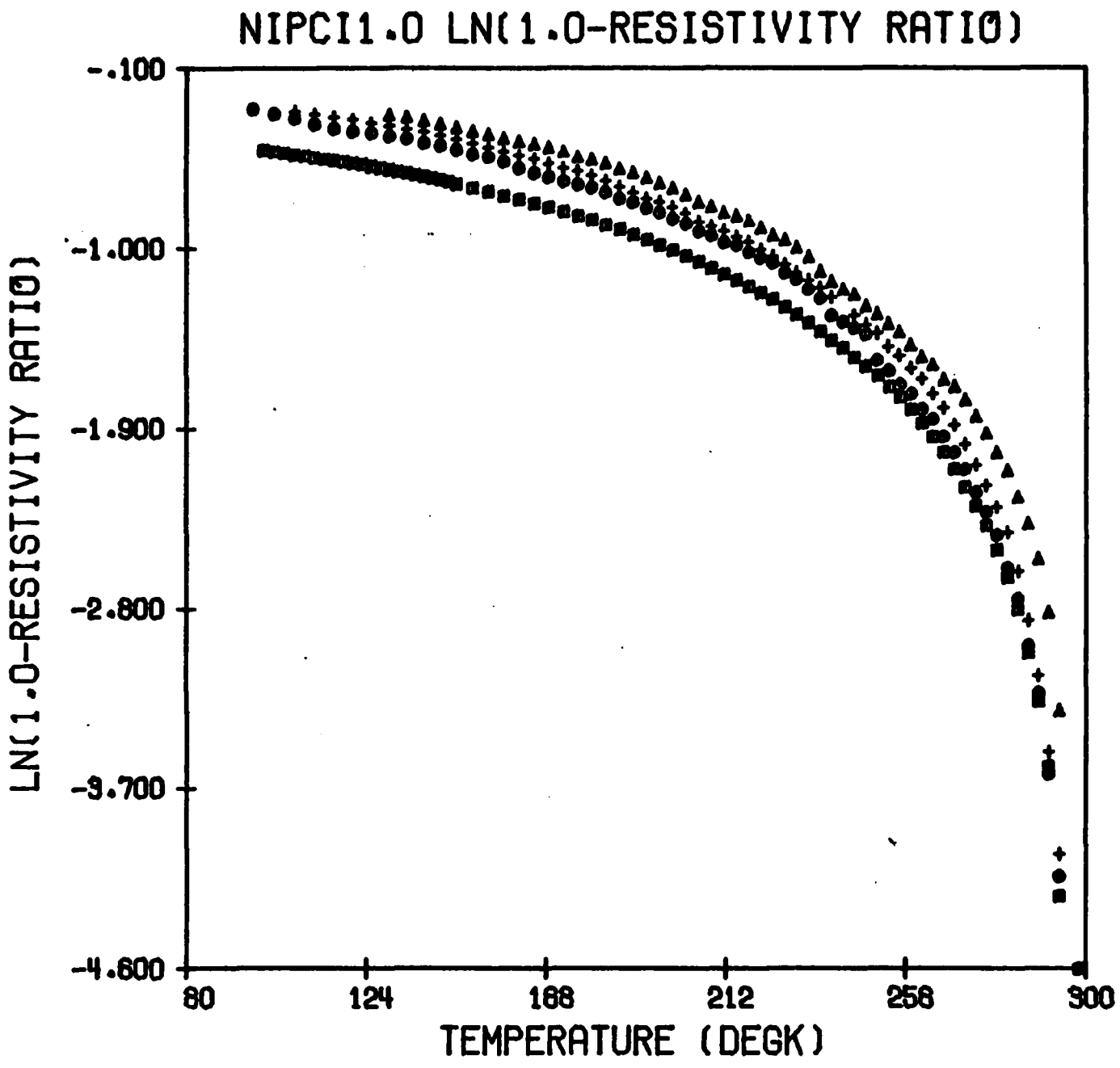
NIPCI1.0 LN(1.0-RESISTIVITY RATIO)
-.100
-1.000
-1.900
-2.800
-3.700
-4.600
LN(1.0-RESISTIVITY RATIO)
80
124
168
212
256
300
TEMPERATURE (DEGK)

P4-2/A23

472:GAN:716:ta
78u472-608

TECHNICAL REPORT DISTRIBUTION LIST, GEN

	No. Copies
Office of Naval Research Attn: Code 472 800 North Quincy Street Arlington, Virginia 22217	2
ONR Branch Office Attn: Dr. George Sandoz 536 S. Clark Street Chicago, Illinois 60605	1
ONR Branch Office Attn: Scientific Dept. 715 Broadway New York, New York 10003	1
ONR Branch Office 1030 East Green Street Pasadena, California 91106	1
ONR Branch Office Attn: Dr. L. H. Peebles Building 114, Section D 666 Summer Street Boston, Massachusetts 02210	1
Director, Naval Research Laboratory Attn: Code 6100 Washington, D.C. 20390	1
The Assistant Secretary of the Navy (R,E&S) Department of the Navy Room 4E736, Pentagon Washington, D.C. 20350	1
Commander, Naval Air Systems Command Attn: Code 310C (H. Rosenwasser) Department of the Navy Washington, D.C. 20360	1
Defense Documentation Center Building 5, Cameron Station Alexandria, Virginia 22314	12
Dr. Fred Saalfeld Chemistry Division Naval Research Laboratory Washington, D.C. 20375	1
U.S. Army Research Office Attn: CRD-AA-IP P.O. Box 1211 Research Triangle Park, N.C. 27709	1
Naval Ocean Systems Center Attn: Mr. Joe McCartney San Diego, California 92152	1
Naval Weapons Center Attn: Dr. A. B. Amster, Chemistry Division China Lake, California 93555	1
Naval Civil Engineering Laboratory Attn: Dr. R. W. Drisko Port Hueneme, California 93401	1
Department of Physics & Chemistry Naval Postgraduate School Monterey, California 93940	1
Dr. A. L. Slafkosky Scientific Advisor Commandant of the Marine Corps (Code RD-1) Washington, D.C. 20380	1
Office of Naval Research Attn: Dr. Richard S. Miller 800 N. Quincy Street Arlington, Virginia 22217	1
Naval Ship Research and Development Center Attn: Dr. G. Bosmajian, Applied Chemistry Division Annapolis, Maryland 21401	1
Naval Ocean Systems Center Attn: Dr. S. Yamamoto, Marine Sciences Division San Diego, California 91232	1
Mr. John Boyle Materials Branch Naval Ship Engineering Center Philadelphia, Pennsylvania 19112	1

P4-2/A25

472:GAN:716:ca
78u472-608

TECHNICAL REPORT DISTRIBUTION LIST, GEN

	No. Copies
Dr. Rudolph J. Marcus Office of Naval Research Scientific Liaison Group American Embassy APO San Francisco 96503	1
Mr. James Kelley DTNSRDC Code 2803 Annapolis, Maryland 21402	1

472:GAN:716:abc
78u472-608

TECHNICAL REPORT DISTRIBUTION LIST, 053

	No. Copies
Dr. R. N. Grimes University of Virginia Department of Chemistry Charlottesville, Virginia 22901	1
Dr. M. Tsutsui Texas A&M University Department of Chemistry College Station, Texas 77843	1
Dr. M. F. Hawthorne University of California Department of Chemistry Los Angeles, California 90024	1
Dr. D. B. Brown University of Vermont Department of Chemistry Burlington, Vermont 05401	1
Dr. W. B. Fox Naval Research Laboratory Chemistry Division Code 6130 Washington, D.C. 20375	1
Dr. J. Adcock University of Tennessee Department of Chemistry Knoxville, Tennessee 37916	1
Dr. A. Cowley University of Texas Department of Chemistry Austin, Texas 78712	1
Dr. W. Hatfield University of North Carolina Department of Chemistry Chapel Hill, North Carolina 27514	1
Dr. D. Seyferth Massachusetts Institute of Technology Department of Chemistry Cambridge, Massachusetts 02139	1
Professor H. Abrahamson University of Oklahoma Department of Chemistry Norman, Oklahoma 73019	1
Dr. M. H. Chisholm Department of Chemistry Indiana University Bloomington, Indiana 47401	1
Dr. B. Foxman Brandeis University Department of Chemistry Waltham, Massachusetts 02154	1
Dr. T. Marks Northwestern University Department of Chemistry Evanston, Illinois 60201	1
Dr. G. Geoffrey Pennsylvania State University Department of Chemistry University Park, Pennsylvania 16802	1
Dr. J. Zuckerman University of Oklahoma Department of Chemistry Norman, Oklahoma 73019	1
Professor O. T. Beachley Department of Chemistry State University of New York Buffalo, New York 14214	1
Professor P. S. Skell Department of Chemistry The Pennsylvania State University University Park, Pennsylvania 16802	1
Professor K. M. Nicholas Department of Chemistry Boston College Chestnut Hill, Massachusetts 02167	1
Professor R. Neilson Department of Chemistry Texas Christian University Fort Worth, Texas 76129	1
Professor M. Newcomb Texas A&M University Department of Chemistry College Station, Texas 77843	1